Validation of Calculated Tissue Maximum Ratio (TMR) Obtained from Measured Percentage Depth Dose (PPD) Data for High Energy Photon Beam (6 MV and 15 MV)

A thesis presented to the:

DEPARTMENT OF MEDICAL PHYSICS

SCHOOL OF NUCLEAR AND ALLIED SCIENCES

UNIVERSITY OF GHANA

BY

JOSEPH EDMOND OSEI

BSc. (KNUST), 2009

10443215

In partial fulfillment of the requirements for the degree of:

MASTER OF PHILOSOPHY

IN

MEDICAL PHYSICS

JULY, 2015

DECLARATION

This thesis is the result of research work undertaken by Joseph Edmond Osei in the Department of Medical Physics, School of Nuclear and Allied Sciences, University of Ghana, under the supervision of Prof. A. K. Kyere, Prof. Cyril Schandorf and Mr. Samuel Nii Adu Tagoe.

…… Date:……..

JOSEPH EDMOND OSEI

(STUDENT)

…….. Date:……..

PROF. CYRIL SCHANDORF

(PRINCIPAL SUPERVISOR)

…… Date:……

PROF. A. W. K. KYERE

(CO-SUPERVISOR)

……. Date:……....

MR. SAMUEL NII ADU TAGOE

DEDICATION

To God Most High be all the glory, honour and praise.

This work is dedicated to my parents, Mr. Philip Ofori and Mad. Cecilia Kwagyin, and my lovely wife Barbara Osei-Duku for having provide me with rich education and fulfilling my spiritual needs throughout their immeasurable support, encouragement love, care and prayers.

ACKNOWLEDGEMENT

I would like to express my utmost gratitude and appreciation to my supervisors Prof. Cyril Schandorf, Prof. A. W. K. Kyere, (Head of Medical Physics Department, School of Nuclear and Allied Sciences, University of Ghana, Legon), for their immeasurable and valuable contributions, guidance, patience, encouragement and suggestions in the preparation of this thesis.

My sincere thanks also goes to Mr. Samuel Nii Adu Tagoe the Medical Physicist, for National Centre for Radiotherapy and Nuclear Medicine (NCRNM) of the Korle-bu Teaching Hospital, Accra, for his huge guidance, encouragement and for his immense support toward the experimental techniques set for this thesis work.

I am also grateful to Mr. George Felix Acquah the Medical Physicist and Radiation Protection Officer at Sweden Ghana Medical Centre, Accra for his time and support and for making their facilities available for this research work.

TABLE OF CONTENTS

LIST OF FIGURES

LIST OF TABLES

LIST OF PLATES

LIST OF ABBREVIATION

2D-XRT	Two Dimensional X-ray Radiotherapy
3D	Three Dimensional
3D-CRT	Three Dimensional Conformal Radiation Therapy
BJR	British Journal of Radiology
BSF	Back Scatter Factor
CCU	Common Control Unit
Co-60	Cobalt-60
CT	Computer Tomography
DC	Direct Current
DICOM	Digital Imaging and Communications In Medicine
EBT	External Beam Radiotherapy
EORTC	European Organisation of Research and Treatment of Cancer
ESTRO	European Society for Radiology and Oncology
HVL	Halve-Value Layer
IAEA	International Atomic Energy Agency
IBA	Ion Beam Application

IEC	International Electro technical Commission
IGRT	Image Guided Radiation Therapy
IMRT	Intensity Modulated Radiotherapy
LC	Liquid Crystal
LET	Linear Energy Transfer
LINAC	Linear Accelerator
MCU	Main Control Unit
MRI	Magnetic Resonance Imaging
NCR	National Research Council
PDD	Percentage Depth Dose
PET	Positron Emission Tomography
PSF	Peak Scatter Factor
PSI	Pacific Semiconductors Industries
PTW	Physikalisch-Technische Werkstatten
RA	Regulatory Authority
RD	Relative Difference
RF	Radio-Frequency

RFA	Radiation Field Analyzer
SAD	Source to Axis Distance
SBRT	Stereotactic Body Radiation Therapy
SCU	Smart Control Unit
SF	Scatter Factor
SGMC	Sweden Ghana Medical Centre
SRS	Stereotactic Radiosurgery
SSD	Source to Surface Distance
TAR	Tissue Air Ratio
TBI	Total Body Irradiation
TMR	Tissue Maximum Ratio
TPR	Tissue Phantom Ratio
TPS	Treatment Planning System
VMAT	Volumetric-Modulated Arc Therapy
WF	Wedge Factor
WHO	World Health Organisation

LIST OF SYMBOLS

%	percentage
μ	linear attenuation coefficient
A	ampere
A_m	field area of maximum dose
C	coulomb
cm	centimeter
cm^2	square centimeter
C_R	reference field size
d_m	depth of maximum build-up
D_m	dose at point at depth of maximum build-up
D_{max}	maximum absorbed dose
D_p	dose at point p
D_t	dose at point t
G.m	gray minute
Gy	gray
Gy/min	gray per minute

hv	energy of a photon
hv_{max}	maximum photons energy
Kev	kilo electron volt
K_s	scattering component
K_{TP}	Pressure-Temperature correction factor
MeV	mega electron volt
mm	millimeter
mm/s	millimeter per second
MV	mega volt
^oc	degree Celsius
R	roentgen
S_c	collimator scatter factor
S_{cp}	total scatter factor
S_p	phantom scatter factor
Z	depth
Z_{max}	point of maximum dose
Z_R	reference depth

ABSTRACT

During external beam radiotherapy treatments, high doses are delivered to the cancerous cell. Accuracy and precision of dose delivery are primary requirements for effective and efficiency in treatment. This leads to the consideration of treatment parameters such as percentage depth dose (PDD), tissue air ratio (TAR) and tissue phantom ratio (TPR), which show the dose distribution in the patient. Nevertheless, tissue air ratio (TAR) for treatment time calculation, calls for the need to measure in-air-dose rate. For lower energies, measurement is not a problem but for higher energies, in-air measurement is not attainable due to the large build-up material required for the measurement. Tissue maximum ratio (TMR) is the quantity required to replace tissue air ratio (TAR) for high energy photon beam. It is known that tissue maximum ratio (TMR) is an important dosimetric function in radiotherapy treatment. As the calculation methods used to determine tissue maximum ratio (TMR) from percentage depth dose (PDD) were derived by considering the differences between TMR and PDD such as geometry and field size, where phantom scatter or peak scatter factors are used to correct dosimetric variation due to field size difference. The purpose of this study is to examine the accuracy of calculated tissue maximum ratio (TMR) data with measured TMR values for 6 MV and 15 MV photon beam at Sweden Ghana Medical Centre. With the help of the Blue motorize water phantom and the Omnipro-Accept software, PDD values from which TMRs are calculated were measured at 100 cm source-to-surface distance (SSD) for various square field sizes from 5x5 cm to 40x40 cm and depth of 1.5 cm to 25 cm for 6 MV and 15 MV x-ray beam. With the same field sizes, depths and energies, the TMR values were

measured. The validity of the calculated data was determined by making a comparison with values measured experimentally at some selected field sizes and depths. The results show that; the reference depth of maximum dose (d_{max}) were 1.5 cm for both PDD and TMR at 6 MV and 2.5 cm and 2.6 cm for PDD and TMR at 15 MV respectively. The minimum relative percentage differences recorded were 1.6 % for 40x40 cm field size and 1.2 % for 5x5 cm field size at 6 MV and 15 MV respectively, while the maximum relative percentage differences recorded were 2.0 % for 10x10 cm field size and 1.4 % for 40x40 cm at 6 MV and 15 MV x-ray beam respectively. The relative differences between the calculated and the measured TMRs increases with depth at all field sizes. It can be concluded that; although based on the results the general agreement between the calculated and measured TMRs is good but for clinically high energy photon beam, it is required that TMR should be measured directly especially when treating deep internal tumor. However it is recommended that comparison of the measured TMR and PDD with that obtained during commission, should be included in the annual quality assurance (QAs) of the machine at SGMC.

CHAPTER ONE

INTRODUCTION

1.1 Background

After x-rays and gamma rays were respectively discovered by Roentgen in 1895 and Paul Villard in 1900, ionization radiations have been applied in many areas of industry and medicine to the benefit of mankind [L'Annunziata et al., 2007]. According to Gamage et al., (2003), though high energy radiations are beneficial, they may be detrimental depending on the mode of application. Clinical use of high energy radiation such as gamma rays, x-rays and other sub-atomic particles to eradicate or manage cancerous cells or tumor (abnormally proliferating cells) is called radiotherapy. Radiotherapy is one of the treatment modalities which is used in the treatment of cancer. It is sometimes use to complement the other treatment options or modalities such as surgery and chemotherapy. Surgery is used for the bulk removal of the tumor that are easily accessible. Chemotherapy is the use of drugs to control the growth of cancerous cells, which is mostly used when there are indications of tumor infiltrating into other neighbouring tissues or there are possible metastases. Since cancerous cells are not easily distinguishable from normal tissue, there is the possibility of leaving traces of cancerous cells behind during surgery, and if these cancerous cells are not taking care off with radiotherapy, there is high tendency of tumor recurrence.

Radiotherapy is categorized into three types based on the mode of administration of the radiations. The three types are; external beam radiotherapy, brachytherapy (or sealed source therapy) and unsealed source therapy. In external beam radiotherapy (EBRT), the source of radiation is remote from the patient who is being treated and the radiation is directed onto be patient through the use of radiation producing machines fitted with collimators [Lawrence et al., 2008]. For brachytherapy the radiation source is placed directly into the tumour (target volume) or in close proximity to the tumour through surgical means or appropriate cavities found in the human body. In unsealed source therapy, substances which certain organs within the human body have high affinity for, are tagged with radioactive agents and are given to the patient intravenously or by oral means. The selection of the substance depends on the target organ within which the tumour is located. A favourable outcome of radiotherapy depends on how best the radiation was able to be optimized to the intended target under treatment and the amount of radiation dose (energy deposited per unit mass) delivered to the target considering all necessary constrains. The advent of computers and sophisticated imaging modalities has revolutionized the practice of radiotherapy. Computers and imaging modalities have been introduced into radiotherapy to assist with the radiation dose optimization process.

It is therefore imperative to know to a high degree of accuracy the radiation dose distribution within the patient undergoing radiotherapy. Placing radiation detectors inside the patient to measure the doses is practically impossible.

Dosimetric functions obtained through beam data measured in water are used to try and link these beam data to what would be pertaining in the patient for EBRT

[Podgorsak, 2006]. The dosimetric functions are influenced by treatment parameters such as; field size, treatment depth, skin to surface distance (SSD) and beam energy (or beam quality). Dosimetric functions are usually determined for square field sizes, and through the concept of equivalent square field size, dosimetric functions of rectangular and irregular fields may be found [ESTRO, 2001]. There are numerous of these functions used in external beam radiotherapy. Among these functions include: tissue air ratio (TAR), percentage depth dose (PDD), peak or back scatter factor (PSF) or (BSF), tissue maximum ratio (TMR), tissue phantom ratio (TPR), scatter factor (Sp) and wedge factor (WF)

Percentage depth dose (PDD) being one way to characterize dose in a patient, is defined as the ratio of the absorbed dose at a given depth in a medium to the absorbed dose at a reference point, expressed as a percentage along the central axis of the beam [BJR, 1996]. It adequately shows how doses are distributed along the beam central axis for a fixed SSD, which is used for monitor unit (or treatment time) calculation in fixed SSD treatment technique. Monitor unit calculation with SSD technique along the central axis is never a problem with PDD, but for treatment where SSD changes from the single SSD, a correction factor called Mayneord F factor may be applied to estimate PDDs for the required SSD [Dawson, 1976]. This method is cumbersome and overestimates the PDDs.

With reference to this, dosimetric function similar to PDD but independent of SSD was introduced for treatment where SSD changes per radiation portal, such as Isocentric or fixed source to axis distance (SAD) technique as well as rotational therapy. In these treatment techniques, the isocenter of the radiotherapy machine

which is mounted isocentrically, is placed in the center of the target volume and the gantry rotated around the patient. SSD changes as the gantry rotates around the patient based on the position of the target within the host, and hence the use of PDD becomes inappropriate for these treatment techniques. John et al., (1953) introduced a dosimetric function called tissue air ratio (TAR) which was originally called tumor air ratio for rotational therapy. TAR is defined as the ratio of the dose at a given point in a phantom to the dose of small mass of water in air at the same point. It depends on the depth in the phantom and field size for a given beam energy.

For a low energy beam where scatter is predominant, TAR is very useful, but for a high energy megavoltage beam, the dose to the small mass of water in air in the definition of TAR is not attainable. In 1965, Karzmark et al. proposed another function called tissue phantom ratio (TPR), which is defined as the ratio of the dose at the isocenter in a phantom for a required depth to that at a reference depth at the same point in the phantom along the beam central axis for a particular field size and beam energy.

1.2 Statement of problem

The concept of tissue-maximum ratios (TMR) as a basis of dose computation has brought problems when applied to a whole range of clinically used megavoltage beams. High energy photon beams exhibit a real variations in their TMR as a function of source-to-axis distance (SAD), but for lower energy treatment units, tissue

maximum ratios (TMRs) exhibit high independence of source-to-axis distance (SAD) [Thomadsen et al., 1992]

However, the calculation method used for the determination of tissue maximum ratio (TMR) from percentage depth dose (PDD) was achieved by emphasizing on differences between TMR and PDD such as geometry and field size, but phantom scatter factors (or peak scatter factors), are introduced to account for the dosimetric variations with field size or collimator settings [Kinsey et al., 2012].

Monitor units and complete dose distributions are nowadays usually computed with treatment planning systems. The dose calculation algorithms and the dose computation procedures in such systems are often not completely known to the user. The accuracy in these computations must be tested by the local physics staff by performing dose measurements in phantoms for typical irradiation geometries.

The method of calculating TMR from PDD data have been found to be in agreement with measured TMR values for low energy (cobalt-60 to 4 MV) megavoltage beams, but not much has been done to validate this for higher megavoltage energy beams. The purpose of this thesis is to compare TMR obtained experimentally and those calculated from PDD data for 6 MV and 15 MV beams from Elekta Synergy Platform linear accelerator, and to come out with recommendations if it is still prudent way of deriving TMR from PDD for these beam energies.

1.3 Objectives

The main objective of this study is to check the validity of tissue maximum ratio (TMRs) calculated from percentage depth dose data for high megavoltage photon beam. TMRs are used in calculating treatment time for patient undergoing isocentric treatment technique for external beam radiotherapy. It is also used by the treatment planning system for dose computation and it is a requirement by the vender of the Oncentra treatment planning system at SGMC where this study was conducted to input TMR measured values for various field sizes and depth for various energy during commission.

The specific objectives are:

- To measure PDD and other dosimetric functions that will enable us to calculate TMR.
- To measure TMR for various field sizes, treatment depths and beam energies
- To calculate TMR values from the measured PDD data and the other dosimetric function
- To compare the calculated TMR with the measured counterpart.
- To compute the percentage difference between the two and see if they are within tolerance of 2%

1.4 Relevance and justification

The treatment of patients using radiotherapy may involve uncertainties (such as, wrong calibration of radiation equipment, misinterpretation of results, patient

movements, and miscalculation of dosimetric quantities) which can lead to severe complications. For this reason, dose must be delivered with the greatest accuracy. Moreover, a small error in the TMR can run through the treatment planning system (TPS) and create systematic error in all the treatments that may be planned with the treatment planning system. The relevance of this work also aims at building a confidence level in the use of the formula for calculating TMR so that it can be used as a second check any time PDD, TMR values are to be measured since there could be error from the equipment used with time.

1.5 Scope and delimitation

The research work will involve the validation of tissue maximum ratio (TMR) calculated from percentage depth dose (PDD) with measured tissue maximum ratio (TMR) data for high energy photon beam at Sweden Ghana Medical Centre (SGMC). This research work will be limited to 6 MV and 15 MV since these are the only highest megavoltage beams available in the country at the time of conducting this research work. Data was taken at SGMC because it is the only oncology centre with these high energy beams and also having a motorized water phantom capable of measuring TMR.

1.6 Organization of thesis

The thesis is arranged in a chronological order of five chapters. Chapter one provides an introduction including problem statement, objectives, relevance and scope of the study. Chapter two reviews the existing literature relevant to the research problem.

Chapter three focuses on the materials and the analytical techniques used in the study. The results obtained are presented and discussed in chapter four. Conclusion of the study, recommendations and suggestions for further study are presented in chapter five.

CHAPTER TWO

LITERATURE REVIEW

This chapter reviews the relevant literatures on tissue maximum ratio, percentage depth dose, the external beam radiotherapy, linear accelerator.

2.1 Background

Dated from the time of Wilhelm Conrad Roentgen (German physicist in 1895) and Henry Antoine Becqueral (French physicist in 1896) who discovered x-rays and radioactivity respectively, applications of ionization radiations in medicine have gone through tremendous transformation. Therapeutic use of ionization radiations started when tissue damage was experienced on the skin after prolonged exposure to x-rays. In 1895, soon after Roentgen's discovery, Leopold and Eduard proposed the use of x-rays for the treatment of diseases [Williams, 1902]. Nowadays, new treatment modalities such as intensity modulated radiation therapy (IMRT) and image guided radiation therapy (IGRT) with very promising treatment outcome have been developed to improve on the quality of life of patients who are candidates for radiotherapy. Imaging modalities such as computer tomography (CT), positron emission tomography (PET) and single positron emission computed tomography (SPECT) are widely and extensively used in radiotherapy to enhance visualization of the tumor for effective targeting of the tumor during treatment delivery.

Radiotherapy, being a treatment modality for controlling tumors, uses high energy radiation to kill cancerous cells [Lawrence et al., 2008]. In using external beam

radiotherapy as treatment modalities, there are many factors to be considered such as the energy of the incident photon, the treated medium (tissue), the treatment technique such as source to surface distance (SSD) and source to axis distance (SAD). All these are carefully considered to ensure maximum accuracy and precision in tumor control probability.

The primary priority in the field of radiotherapy is to accurately deliver dose to the targeted volume and sparing the surrounded normal tissues. This as stated by ESTRO, 2001 that there is only 3.5 % allowable tolerance required as a standard in dosimetry. This figure is the total uncertainty and is stated as one standard deviation of the dose value at a specified point or in the mean dose to the target volume [Wambersie et al., 1994]. For such a high accuracy to be maintained, it was suggested by working group in the European Organization of Research and Treatment of Cancer (EORTIC) that, some levels must be adopted [Johansson et al., 1986]. These include; $\pm$ 3 % allowable deviation when calibrating a therapy units and $\pm$ 5 % allowable deviation when delivering a prescribed dose (especially when dose characteristics, shielding blocks, trays, wedges or other non-reference conditions are involved). With some treatments, lower tolerance is needed [Brahme, 1988]. Work is, however, ongoing to enhance the dosimetry accuracy.

Notwithstanding, to accurately delivery a dose to a targeted volume, the distribution of dose in the medium must precisely be known [AAMP, 1983]. Direct measurements of dose distribution is quite unattainable but several functions such as PDD, TAR, TMR and BSF can be used to connect the dose at an arbitrary point to an already known dose at the calibration point in the phantom [Podgorsak, 2006]. Percentage depth dose

being one of the common dosimetric functions is applicable to only source to surface distance (SSD) technique. As clearly stated in BJR supplement 25 that, PDD data are always not attainable in many occasions, especially, when using SAD technique, another dosimetric function should be investigated. Johns et al., (1953) then elaborated on replacing PDD with TAR so as to provide room for isocentric (SAD) treatment technique. Moreover, many errors such as improper positioning of ion chamber, representation of ionization by depth dose and wrong normalization of peak depth dose are incurred when taking PDD measurements [BJR, 1996]. Since TAR involves in-air measurements, very large build-up cap is needed for electronic equilibrium when using high megavoltage beams. This calls for the modifications of dose factors or output factors or calibration factors when changing from the use of low energy photon beam for treatment, to a high energy photon beam. To circumvent these problems, tissue maximum ratio (TMR) was introduced.

2.1.1 Origin of Tissue Maximum Ratio (TMR)

[Karzmark et al.,1965] explained the need to replace tissue air ratio by a new ratio which they called the tissue phantom ratio (TPR) and to restrain from air measurement for a calibration procedure common to all energies and all types of radiations. The tissue phantom ratio (TPR) was defined as the ratio of the dose, (D_t/D_p), under the conditions of electronic equilibrium, where D_p is the dose at a specified point T on the beam axis in a phantom with an underlying material for full backscatter, and D_t is the dose at the same spatial point T but with an arbitrary depth t of overlying tissue [Agarwal et at., 1971]. In 1970, Holt et al. came up with another concept, tissue

maximum Ratio (TMR), to expatiate the usefulness of tissue air ratio (TAR) to high megavoltage beams and experimented with 6 MV x-rays. Tissue maximum ratio (TMR), at point p at a depth d where the field size is 'A' was defined as the ratio of the dose in the irradiated medium at a point at depth d, to the dose at the same spatial depth p in a phantom of the same medium with infinite lateral extent and at a depth just sufficient to provide maximum dose build-up [Cunningham et al., 1965].

2.1.2 The Need to Measure Tissue Maximum Ratio

When high energy photon beams were not common, tissue air ratio (TAR) was defined for low x-ray energies. The TMR is a variation of the TAR that makes it suitable for use at high energies. TAR and TMR are similar, but not identical concepts because the reference depth for TMR is the depth of maximum dose (d_{max}) [Edward et al., 2008].

Tissue air ratio (TAR) uses the dose to tissue in air under conditions of minimum tissue absorption and scattering as the reference denominator. Because, high-energy photons introduce large range of secondary electrons, the tissue mass in air satisfying the condition for electronic equilibrium also becomes large, hence measuring more distance in diameter. This large tissue mass can also contribute a considerable amount of scattered photon fluence. With that mass of tissue placed in air, it is incorrect to refer to the reference denominator as a dose in air and the ratio as tissue air ratio. Tissue maximum ratio (TMR) nullifies this problem.

2.2 Factors for Calculating Photon Beam Distribution.

There are many of these functions (dosimetric fundamental quantities) used in external beam radiotherapy. Among these functions include: tissue air ratio (TAR), percentage depth dose (PDD), peak or back scatter factor (PSF) or (BSF), tissue maximum ratio (TMR), tissue phantom ratio (TPR), scatter factor (Sp) and wedge factor (WF).

2.2.1 Percentage Depth Dose (PDD)

Percentage depth dose (PDD) is defined as the ratio of the dose at any depth (d) in a phantom to the maximum dose at reference depth. It is a common dosimetric function to characterize the variation of absorbed dose in a patient (phantom) with depth along the axis of the beam. It uses the source to surface (skin) distance (SSD) technique in treatment. Percentage depth dose (PDD) depends on many factors such as the quality of the beam or energy, the depth of treatment, the field size, and the source to surface distance. It shows a proportional decrease with depth for all energies beyond build -up region but increases with energy beyond build-up region [Mayneord and Lamerton, 1941].

According to Subramania and Lawrence, 2001, for a constant beam energy, PDD increases with field size, because of the larger area from which radiation can be scattered. PDD again increases with SSD because of the effect of beam divergence. The PDD allows monitor units to be calculated when the point of calculation is not z_{max}, where z_{max} is the point of maximum dose [Buono, 2010].

2.2.2 Tissue Air Ratio (TAR)

Tissue air ratio is the ratio of the dose at depth in a tissue to the dose in air (that is, small tissue situated in air surrounded by just enough material to generate electronic equilibrium) at the same distance from the source and the same field size. In the olden days, when backscatter factor was defined as the ratio of exposure on the surface of an irradiated medium to the exposure at the same distance from the source, (Johns et al, 1953) also explained TAR to be a ratio of exposure at a point in a phantom to the exposure in air at the same distance from the source. This implies that, TAR on the surface of a patient can be called backscatter factor (BSF).

Since BSF considered at the reference depth of maximum dose changes into peak scatter factor (PSF), the use of exposure in its definition was changed into absorbed dose [ICRU, 1973]. This led to redefining TAR by the use of absorbed dose instead of exposure (according to ICRU report 23), but because it is conceptually simple and unclear, various attempts have been made to redefine the quantity [BJR, 1983, Khan, 1984]. According to ICRU report 23, TAR is defined as the ratio of absorbed dose at a point in a phantom to the absorbed dose at the same point in free air within a volume of the phantom material, large enough to provide maximum electronic build up at the point of reference [ICRU, 1976]. This definition exhibits many limitations such that, there was no clear specification of the shape and size of the phantom material [Cunningham and John, 1970], no specification of whether contaminated electrons contribute to the absorbed dose for which Henry (1974) lamented on the negligible effect of these electrons. Also, with this definition, derivation of scatter-air ratio for non-uniform and irregular fields becomes a problem [Cunningham, 1972]. With

regards to this discussion, [Pfalzner,1981] proposed that the discrepancy between TAR and PSF could be dealt with by redefining the denominator of TAR.

The TAR is used in isocentric techniques when the point of dose calculation is always at the same distance from the source. It removes the need for an SSD measurement because it is constant for most SSDs used in radiotherapy treatment. Nowadays tissue air ratio is widely used in calculation involving isocentric treatment time for low energy radiation beam, but has a hidden problem at higher energies. TAR is therefore not applicable to modern linear accelerators due to concerns with build-up in the air measurement [Buono, 2010].

2.2.3 Tissue Phantom Ratio (TPR)

Tissue phantom ratio (TPR) is the ratio of the dose at depth z to that at reference depth Z_R in water equivalent phantom for the same collimator setting and source-detector distance. It is a function of depth z, field size s at depth z, and reference depth Z_R [ESTRO, 2001].

TPR is a general function that may be normalized to any reference depth. Actually, there is no uniform agreement concerning the reference depth to be used for this quantity, the point of central axis d_{max} has an uncompounded characteristic that is very useful in dose computations [Samulski et al., 1981]. If d_{max} is adopted as a fixed reference depth, the quantity TPR changes to the tissue maximum ratio (TMR)

TPR allows correction of monitor units or treatment time to be accounted for, if a change in dose at depths other than the reference are used. It is an SAD dependent and

this makes it have an advantage over percentage depth dose measurements which are dependent on source to surface distance (SSD).

2.2.4 Tissue Output Ratio

Tissue output ratio is the ratio of the dose at depth z, for field size s, to the dose at the reference depth $Z_{R,}$ for a reference field size C_R, at the same source-detector distance. Tissue output ratio involves both phantom scatter and head scatter, and these components have to be separated in calculating monitor units for complex situation.

2.3 Equivalent Square Field

Many dosimetric functions such as PDD, TAR, TMR and BSF are functions not only of energy of the photon beam and depth but also the size and shape of the incident field. Shape of radiation fields are thus, standardized to either circular or square fields so as to obtain agreeable tables of data [BJR, 1996].

Equivalent square field, as defined by [Jones, 1949 and Day, 1950] as a standard (square) field with the same central axis depth dose characteristics as that given in non-standard field.

Based on previous works on equivalent square field by Sterling et al., (1964), two other scientists; Worthley (1966) and Patomaki (1968) established that, the equivalent square field can be calculated from the so-called ‘4xArea / perimeter or 4A / P’ as

$$\sigma = \frac{4ab}{2(a+b)} \quad 2.1$$

$$\sigma = \frac{2ab}{(a+b)} \quad 2.2$$

where σ is the side of the equivalent square, 'a' and 'b' are the sides of the rectangle. This equation works very well for smaller rectangles, with side 'a' or 'b' less than or equal to 20 cm.

2.4 External Beam Radiation Therapy

External beam radiotherapy (EBT) also called external radiation therapy or teletherapy is a type of radiation therapy that uses a machine to direct high energy ionizing rays to a tumor from outside the body. During external beam radiation therapy, a beam of radiation is directed through the skin to the tumor and the immediate surrounding area in order to destroy the main tumor and any nearby cancerous cells. To achieve this, and minimize the radiation effect on the normal tissue, the treatments are fractionated for a number of weeks. Patients usually receive external beam radiation therapy in daily treatment sessions over the course of several weeks. The number of treatment sessions depends on many factors, including the total radiation dose that will be given. This allows enough radiation to be available in the body to kill the cancerous cells while giving the healthy cells time, each day, to recover.

External beam radiation therapy is most often delivered in the form of photon beams (either x-rays or gamma rays). A photon is the basic unit of light and other forms of electromagnetic radiation. It can be thought of as a bundle of energy. The amount of

energy in a photon can vary. The photons in gamma rays have the highest energy, followed by the photons in x-rays. These radiation beams can be generated by ^{60}Co machine, which produces gamma radiation or linear accelerator (also known as LINAC), producing high-energy x-rays beam. A LINAC uses electrical energy to form a stream of fast-moving subatomic particles. This creates high energy radiation that may be used to treat cancer.

By the help of high technique treatment planning software, the treatment team controls the size and shape of the beam, as well as how it is directed into the body, so as to effectively treat the tumor while sparing the surrounding normal tissue. EBT comes with many types depending on the beam energy, beam size and beam shape. These include: conventional external beam radiotherapy, stereotactic radiation therapy, three-dimensional conformal radiation therapy (3D-CRT), proton beam therapy, image guided radiation therapy (IGRT), particle therapy and neutron beam therapy.

2.4.1 Conventional External Beam Radiotherapy

This is the type of external beam radiotherapy delivered through two-dimensional beams using linear accelerator machines (2DXRT) or cobalt 60. It consists of a single beam of radiation delivered to the patient from several directions: often front or back, and both sides of the patient.

2.4.2 Stereotactic Radiation Therapy.

Stereotactic radiation therapy is a specialized type of external beam radiation therapy that uses a focused radiation beams targeting a well-defined tumor by the help of extremely detailed image scans. Stereotactic radiation therapy comes in two types, namely; Stereotactic body radiation therapy (SBRT) and stereotactic radiosurgery (SRS).

2.4.2.1 Stereotactic Body Radiation Therapy

Stereotactic body radiation therapy (SBRT) delivers high radiation doses in fewer sessions, using smaller radiation fields than 3D-CRT in most cases. By definition, SBRT treats tumors that lie outside the brain and spinal cord. Because these tumors are more likely to move with the normal motion of the body, and therefore cannot be targeted as accurate as tumors within the brain or spine, SBRT is usually given in more than one dose. SBRT is often applicable to the treatment of small, isolated tumors such as cancer in the lungs and liver. It is always referred to by their brand name as CyberKnife [Answers, 2009].

2.4.2.2 Stereotactic Radiosurgery

Stereotactic radiosurgery (SRS) can deliver one or more high doses of radiation to a small tumor. SRS uses extremely accurate image-guided tumor targeting and patient positioning. Therefore, a high dose of radiation can be given without excessive damage to normal tissue. SRS can be used to treat only small tumors with well-defined edges. It is most commonly used in the treatment of brain or spinal tumors and brain metastases from other cancer types. For the treatment of some brain metastases, patients may receive radiation therapy to the entire brain (called whole-brain radiation therapy) in addition to SRS. SRS requires the use of a head frame or other device to immobilize the patient during treatment to ensure that the high dose of radiation is delivered accurately. SRS concentrates a high radiation dose non-invasively; but dosimetric studies have illustrated the possibility of managing early-stage breast cancer with SRS [Wegner, 2011]

2.4.3 Three-Dimensional Conformal Radiation Therapy (3D-CRT)

Three-dimensional conformal radiation therapy **(**3D-CRT) uses very complex computer software and advanced treatment machines to deliver radiation to very precisely shaped tumor target areas. It incorporates special imaging techniques such as computer tomography (CT), magnetic resonance imaging (MRI), positron emission tomography (PET) scans to show the size, shape and location of the tumor as well as the surrounding organs. With multileaf collimator or customized fabricated field-shaping blocks, the radiation beams are directed precisely to the shape and size of the tumor [Answers, 2009].

2.4.4 Intensity Modulated Radiation Therapy

Intensity modulated radiation therapy (IMRT) uses hundreds of tiny radiation beam-shaping devices, called collimators, to deliver a single dose of radiation. The collimators can be stationary or can move during treatment, allowing the intensity of the radiation beams to change during treatment sessions. This kind of dose modulation allows different areas of a tumor or nearby tissues to receive different doses of radiation.

Unlike other types of radiation therapy, IMRT is planned in reverse (called inverse treatment planning) [Purdy, 1996]. In inverse treatment planning, the radiation oncologist chooses the radiation doses to different areas of the tumor and surrounding tissue, and then a high-powered computer program calculates the required number of beams and angles of the radiation treatment. In contrast, during traditional (forward) treatment planning, the radiation oncologist chooses the number and angles of the radiation beams in advance and computers calculate how much dose will be delivered from each of the planned beams.

The goal of IMRT is to increase the radiation dose to the areas that need it and reduce radiation exposure to specific sensitive areas of surrounding normal tissue. Compared with 3D-CRT, IMRT can reduce the risk of some side effects, such as damage to the salivary_glands (which can cause dry mouth, or xerostomia), when the head and neck are treated with radiation therapy. However, with IMRT, a larger volume of normal tissue overall is exposed to radiation. Comparison of IMRT with 3D-CRT as to

whether it provides improved control of tumor growth and better survival is not yet known [Answers, 2009].

2.4.5 Image Guided Radiation Therapy (IGRT)

In image guided radiation therapy (IGRT) repeated imaging scans (CT, MRI, or PET) are performed during treatment period. These imaging scans are processed by computers to identify changes in a tumor's size and location to allow the position of the patient or the planned radiation dose to be adjusted during treatment as needed. Repeated imaging can increase the accuracy of treatment and may allow reductions in the planned volume of tissue to be treated, thereby decreasing the total radiation dose to normal tissue. IGRT as importantly used for curative and palliative treatments, constitutes more than 50 % of all lung cancer treatment modalities [Antink and Bernhard, 2011].

2.4.5.1 Tomotherapy

Tomotherapy is a type of image-guided IMRT. A tomotherapy machine is a hybrid between a CT imaging scanner and an external beam radiation therapy machine. The part of the tomotherapy machine that delivers radiation for both imaging and treatment can be rotated completely around the patient in the same manner as a normal CT scanner. Tomotherapy machines can capture CT images of the patient's tumor immediately before treatment sessions, to allow for very precise tumor targeting and sparing of normal tissue.

Like standard IMRT, tomotherapy may be better than 3D-CRT at sparing normal tissue from high radiation doses. However, no comparison has been made to compare 3D-CRT with tomotherapy [Answers, 2009].

2.4.6 Proton Beam Therapy

External beam radiation therapy can be delivered by proton beams as well as photon beams described above. Protons are type of charged particles. Proton beams differ from photon beams mainly in the way they deposit energy in tissue. Whereas photons deposit their energy in small packets all along their paths through tissue, protons deposit most of their energy at the end of their path (called the Bragg peak) and deposit less energy along the way. In theory, the use of protons should reduce the exposure of normal tissue to radiation, possibly allowing the delivery of higher doses of radiation to a tumor [Answers, 2009].

2.4.7 Neutron Beam Therapy

Neutron beam therapy is a specialized form of external beam radiation therapy. It is often used to treat certain tumors that are radio resistant. Fast neutron can control very large tumors because, unlike low LET (linear energy transfer) radiations, neutrons do not depend on the presence of oxygen to kill cancer cells. The biological impart of neutrons on cells is very great than the other types of ionization radiation [Answers,

2009]. Because the biological effectiveness of neutrons is so high, the required tumor dose to kill cancer cells is about one-third the dose required with that of photons, electrons or protons.

2.5 Photon Beam Sources

Photon sources are either isotropic or non-isotropic and they emit either mono energetic or heterogeneous photon beams. The most common photon sources used in radiation oncology are x-ray machines, teletherapy radio-isotope sources and LINACS.

An isotropic photon source produces the same photon fluence rate in all directions, while the photon fluence rate from a non-isotropic source depends on the direction of measurement. A plot of the number of photons per energy interval versus photon energy is referred to as a photon spectrum.

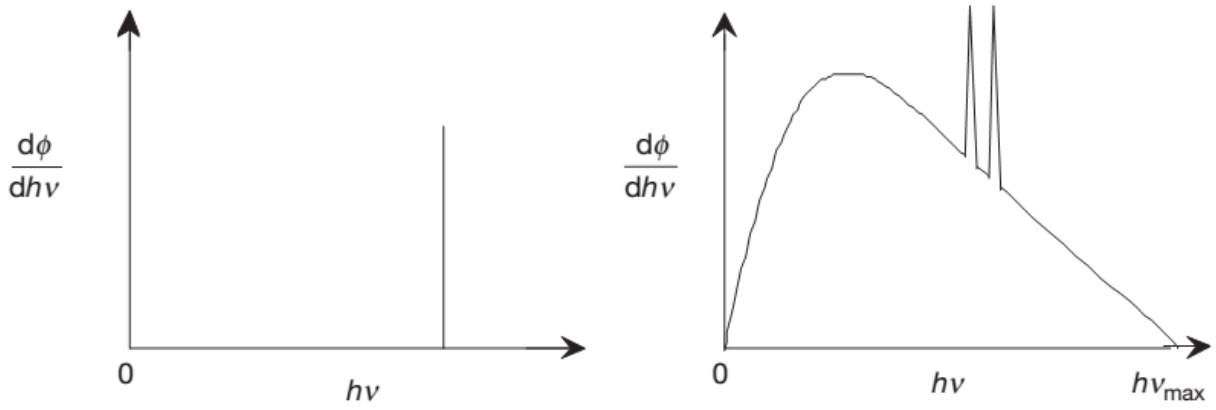

(a) **(b)**

Figure 2.1 Typical spectra1for (a) monoenergeticbeam and (b) heterogeneous photon beam

All photons in a mono energetic photon beam have the same energy. Photons in a heterogeneous x-ray beam form a distinct spectrum, with photons present in all energy intervals from zero to a maximum value, which is equal to the kinetic energy of electrons striking the target. Gamma ray sources are usually isotropic and produce mono-energetic photon beams, while x-ray targets are non-isotropic sources producing heterogeneous photon spectra.

2.5.1 High Energy X-ray Production in Linear Accelerator (LINAC)

One of the most specialized characteristics of a fast-moving electron is that when it interacts with a material, it can produce an x-ray. Part or a whole of the kinetic energy of the electron is transformed into electromagnetic energy. This principle is used to obtain x-rays in most x-ray production machines in which electrons are accelerated and directed to hit a target and then generate an x-ray. The amount of x-ray photon particles produced increases as the kinetic energy of the incident electrons increases. Electrons are accelerated by the potential differences in diagnostic x-ray tubes, up to several hundred kilo-electron volts (KeV). The acceleration mechanism in linear accelerator, however, is somewhat different because it uses microwave technology similar to that used for radar to accelerate electrons in a linear tube, often called accelerator tube.

In linear accelerators, electrons are usually accelerated to the energy range of 4 – 25 MeV. A 6 MeV electron is most often used to create an x-ray for radiosurgery. When an electron creates a photon, theorithecally, the photon can take any energy from zero to a maximum as the same as the energy of the incident electron [Padikal and Deye, 1978]. In other words, the photon beam produced by a 6 Mev electron beam can have

energy spectrum of 0-6 MV. The energy of an x-ray produced in a linear accelerator is denoted by MV. The major components and auxiliary systems of a typical medical linear accelerator are shown in a block diagram in below (fig. 2.2).

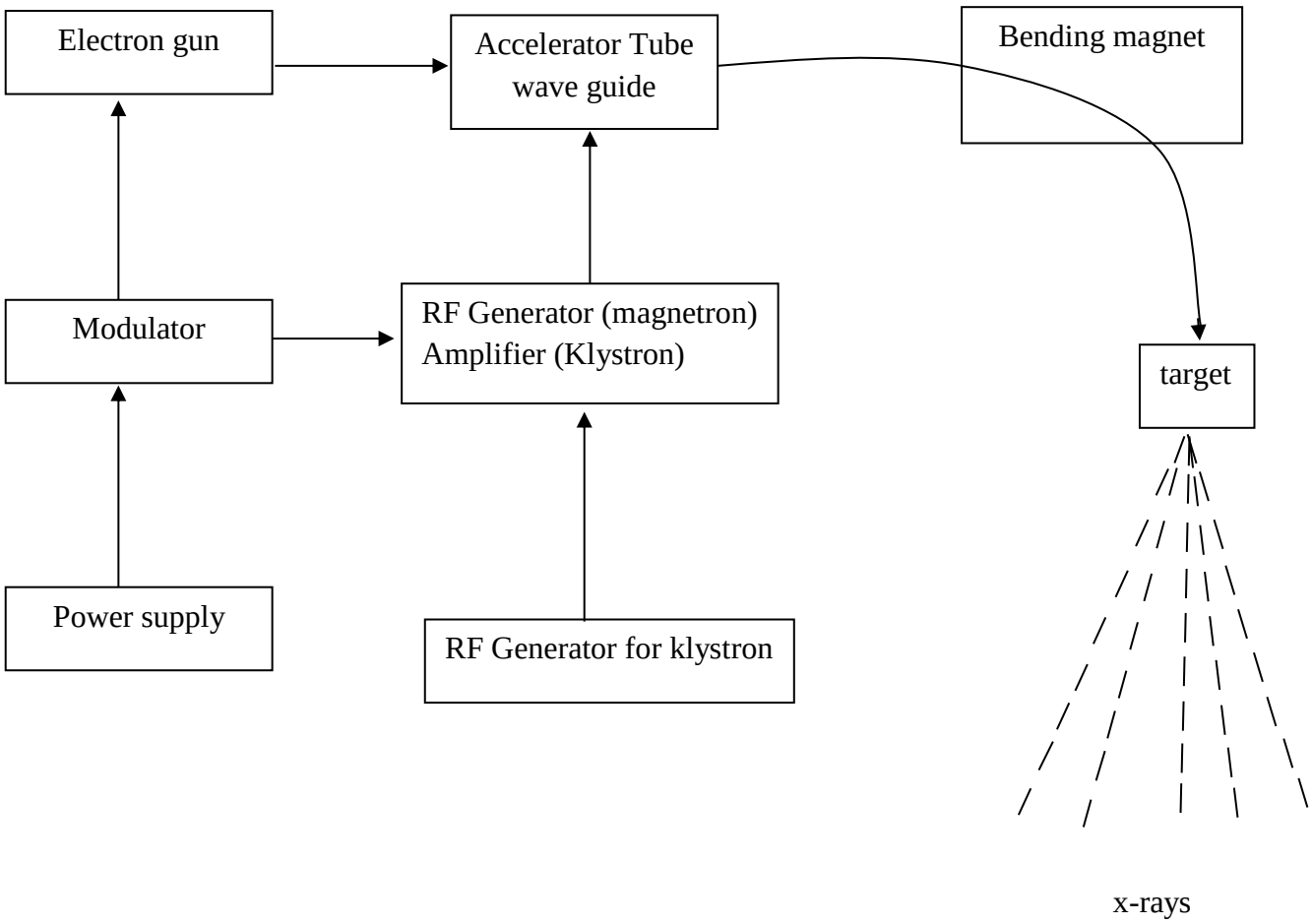

Figure 2.2 A schematic diagram of x-ray production from linear accelerator

The power supply provides DC to the modulator, which provides a high-voltage pulse to the RF generator and the electron gun at the same time. The electron gun introduces the electrons which are produced thermionically in pulse to the accelerator tube. The RF generator produces a microwave to the accelerator tube. The electrons and the

microwave are timed exactly to be met in the accelerator tube by the modulator. The accelerator tube accelerates the electrons. As the accelerated electrons come out of the accelerator tube, the path of the electrons is bent through a bending magnet to hit the target and generate x-rays.

2.5.2 Teletherapy Radioisotope Source (cobalt – 60)

As used in radiotherapy, cobalt units produce stable, dichromatic beams of gamma rays of 1.17 and 1.33 MV, resulting in an average beam energy of 1.25 MV. The cobalt-60 isotope has a half-life of 5.3 years so the cobalt-60 needs to be replaced occasionally. Gamma rays have quite more energy than regular light, and their wavelength is a lot shorter too, these attributes could make them an ideal candidate for better data communications and other physics applications. Unfortunately, they are not as easy to produce as regular light. A common cobalt-60 source is a cylinder of diameter 2 cm, height 5 cm, and is positioned in the cobalt Unit with the circular end facing the patient. The fact that the radiation source is not a point source complicates the beam geometry and produces what is known as the geometric penumbra and the transmission penumbra. These penumbras create a region of dose variation at the field edges. Cobalt-60 gamma radiation typically has energy of about 1.2 MV, depth of maximum dose (Dmax) being 0.5 cm. and a percentage depth of 55 % at 10 cm. Cobalt units with low energy gamma rays are ideal for treatment of head and neck cancers. This would cover 25 % of cancers seen in a large cancer treatment center. Majority of others will be cervical cancers and others like cancers of oesophagus, lung and prostate.

2.6 Review of Works on the Measurement of Percentage Depth Dose (PDD) and the Tissue Maximum Ratio (TMR) in EBT.

Treatment of diseases with radiotherapy presents some risk for the patient, because, an overexposure or an underexposure of patient to radiation can produce more harm than cure to patient and secondly, there is a risk for normal tissue from excessive radiation exposure. Accidents have been occurring in the field of radiotherapy treatment over the years up to date, and they will continue to occur even though, there is advancement of new technologies in radiotherapy. But over years, methods for dose delivery in radiotherapy treatments have been developed and revised so as to prevent and to reduce the errors that cause these accidents. In the year 1997, the IAEA analyzed a series of accident exposures in radiotherapy to draw lessons for the preventions of these occurrences [IAEA, 1997; WHO, 2008]. Many methods such as good treatment planning system (TPS) and good image scan (simulation) have been established to locate and mark the tumor area.

In 1971, Agarwal, Scheele and Wakley worked on tissue maximum ratio for 8 MV x-rays. In their experiment, the validity of the calculated tissue maximum ratio (TMR) was determined by making comparison with values measured experimentally at selected field sizes and depths in water phantom. They showed that, the tissue maximum ratio (TMR) values were not affected significantly by changing source-to-axis distance.

They concluded that; the calculated TMR data compared with the experimental data were in good agreement.

In 2013, Spunei, Mihai and Malaescu worked on the experimental results in percentage depth dose (PDD) determination at the extended distances. In their experiment, experimental results in percentage depth dose (PDD) and tissue maximum ratio (TMR) for large fields at extended distances which could be used for total body irradiation (TBI) technique were compared with those calculated. They concluded that; when TMR data obtained at 180 cm were compared with literature, it was found that the relative difference between measured and literature was within 0.2 % and 3 % [Spuneiet al., 2013].

In 2012, Kinsey, Guerroro, Prado and Yi also performed experiment on the validity of the calculation method for determining tissue maximum ratio (TMR) from percentage depth dose (PDD) for flattening filter-free photon beam. In the experiment, calculated TMR values were compared with measured TMR values using flattening filter-free photon beam. They concluded that for field sizes less 20 cm, no noticeable differences were found down to 30 cm depth. The calculated TMR's started to deviate around 15 cm depth for field sizes larger than 20 cm. The differences increase with depth and field size, leading to a deviation up to 3.2 % [Kinsey et al., 2012].

Bagne, (1974), reported that tissue maximum ratio (TMR) for 33 MV and 45 MV x-ray beams from a betatron exhibited a dependence on the source-to-detector distance, an inherent characteristic not shown by lower-energy photon beams.

Dawson, (1977), gathered Bagne's findings on a similar machine. Bagne, (1974) postulated that, the distance dependence of TMR results from the difference in relative amount of low energy scattered photons (originating from interactions in the

collimators) in the beam at various distances. Welkley et al., (1975), after noticing a shift in the position of peak depth with source-to-skin distance (SSD) for 25 MV betatron beam, suggested contaminant electrons as the cause, as Marinello and D utreix, (1973), had previously suggested for the shift in peak depth with field size.

2.7 Converting Percentage Depth Dose (PDD) into Tissue Maximum Ratio (TMR)

Tissue maximum ratio (TMR) at a point P in a phantom is defined as the ratio of the dose at a point P in an irradiated phantom to the dose at the same spatial point P in the same phantom with infinite lateral extended and overlying thickness just sufficient for maximum build-up. This is shown in fig. 2.3 (a) and fig. 2.3 (b). That is

$$T_{mr}(A_d, \mathrm{d}, \mathrm{E}) = \frac{D_d}{\mathrm{D}_{dm}} \qquad 2.3$$

The symbol D_{dm} represents the dose at point P at the same spatial point in an irradiated phantom but having an overlying thickness of the phantom just sufficient for maximum build-up as shown in figure 2.3 (b). $\mathrm{A_d}$ is the field area at depth d, T_{mr} is the tissue maximum ratio and E denotes the energy of the radiation beam. Hence

$$T_{mr}(A_d, \mathrm{d}, \mathrm{E}) = \frac{D_d}{\mathrm{D}_{\boldsymbol{m}}} \cdot \frac{\mathrm{D}_{\boldsymbol{m}}}{\mathrm{D}_{\mathrm{dm}}} = \frac{Pdd}{100} \cdot \frac{D_m}{D_{dm}} \qquad 2.4$$

Where: D_m is the dose at point Q at depth d_m from the surface of the irradiated phantom in (fig. 2.3 (a)) that is; the dose at the position of maximum build-up and pdd is the percentage depth dose at point P in (figure 2.3 (a)) for the given field size. The position of point Q in (fig. 2.3 (a)) and P in (fig. 2.3 (b)) are the same so far as the phantom is concerned, but P is at a distance F + d from the source, whereas Q is at a distance F + d_m from the source. Applying the inverse square law, and allowing for scatter factors,

$$\frac{D_m}{D_{dm}} = \left(\frac{F+d}{F+d_m}\right)^2 . \frac{S_p(A_m,E)}{S_p(A_d,E)} \qquad 2.5$$

Where; $S_p(A_m, E)$ and $S_p(A_d, E)$ denote the phantom scatter factors corresponding to field areas A_m (at the level of Q) and A_d respectively for fixed collimator setting. Hence,

$$T_{mr}(A_d, \mathrm{d}, \mathrm{E}) = \frac{Pdd}{100} . \left(\frac{F+d}{F+d_m}\right)^2 . \frac{S_p(A_m,E)}{S_p(A_d,E)}$$

2.6

This value of T_{mr} applies to a beam with a field size A_d at depth d, whereas pdd is the percentage depth dose.

The determination of the values of $S_p(A,E)$ was based on inverse square law measurements

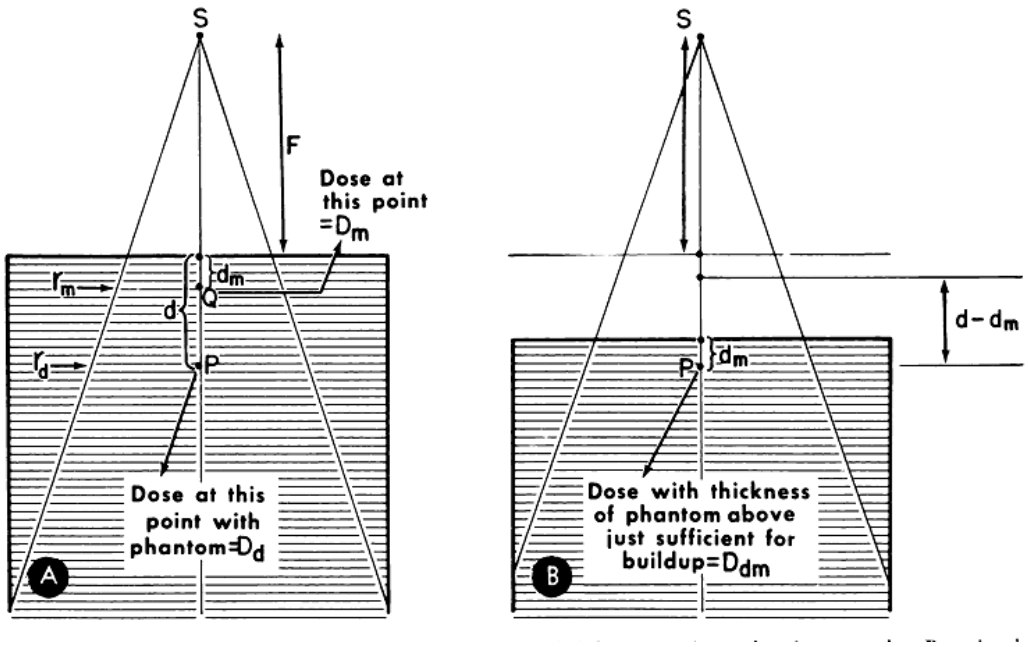

Figure 2.3: (a) Set-up to determine dose at point P at depth d in an irradiated phantom. (b) Set-up to determine dose at point P in the same phantom with infinite lateral extent and overlying thickness just sufficient for maximum build-up.

2.7.1 Phantom Scatter Factor (S_p)

Phantom scatter factor being a ratio of dose rate at reference depth for a given field size to the dose rate at the same depth for a reference field size (10x10 cm), becomes difficult to measure in practice [Khan, 2012]. An indirect method of determining phantom scatter factor (S_p), relates the total scatter factor (S_{cp}) to the collimator scatter factor (S_c) as;

$$S_p(r) = \frac{S_{cp}(r)}{S_c(r)} \qquad 2.7$$

where r is the given field size.

The total scatter factor S_{cp} is obtained from the formula,

$$S_{cp} = \frac{D(S,d_{ref})/M}{D(S_{ref,}\, d_{ref})/M} \qquad 2.8$$

where M is the monitor unit, s is the field of interest, D is the dose, d_{ref} is the reference depth and S_{ref} is the reference field size.

The collimator scatter factor S_c is also determined from the formula,

$$S_c = \frac{K_p(c,Z_{ref})/M}{K_p(c_{ref}\,, Z_{ref}\,)/M} \qquad 2.9$$

Where M is the monitor unit, K_p is the ionization in air, C_{ref} is the reference field size and Z_{ref} is the reference depth.

2.8 The Oncentra MasterPlan Treatment Planning system.

Medical imaging are mainly used to form a virtual patient for computer-aid design procedure. Geometry, radiology and dosimetric aspect of therapy are planned using treatment simulation and optimization [Karabis et al.,2009]. In other for greater modulation to be attained by the intensity of radiation therapy, simulations are done by carefully selecting the required beam energy, beam arrangement, catheter positions and source dwell time [Lahanas et al.,2003]. The more optimization process is formal, the better the process could be referred to as forward planning or inverse planning [Galvin et al., 2004].

Oncentra MasterPlan is a treatment planning system comprising of many individual treatment planning modules for external beam radiation therapy and brachytherapy. Oncentra is designed for DICOM integration, connectivity and flexibility. Oncentra MasterPlan TPS allows numerous sets of data points to be classified as applicator points [Malhotra et al., 2012]. For MasterPlan photon dose calculation, parameters such as energy deposition kernels, electron contamination kernels, fluence matrix, source size, head scatter, ionization chamber perturbation are required. In using TMR value to determine the dose at isocentre (D_{iso}) and the maximum dose at d_{max}, (D_{dmax}), the following equations are used.

$$D_{iso} = mu \times I_{sq} \times TMR \times OF \times CF \quad 2.10$$

$$D_{dmax} = mu \times I_{dmax} \times TMR \times OF \times CF \quad 2.11$$

$$I_{dmax} = \left(\frac{100}{100-d+dm}\right)^2 \quad 2.12$$

Where mu is the monitor unit, I_{sq} is the inverse square correction, TMR is the tissue maximum ratio, OF is the output factor I_{dmax} is the inverse square correction at depth of maximum dose and CF is the calibration factor.

CHAPTER THREE

MATERIALS AND METHODS

This chapter describes the materials and the experimental methods used in this study. The research work was carried out using the Linear Accelerator, Elekta Synergy platform and Blue phantom two water tank system and equipment at the Sweden Ghana Medical Centre (SGMC).

3.1 Materials

The materials used in this study include; the linear accelerator unit, three dimensional motorized water phantom, ionization chamber, electrometer, laptop for data acquisition and distilled water.

3.1.1 The Linear Accelerator (LINAC) used

The radiotherapy unit at Sweden Ghana Medical Centre has one Synergy platform linear accelerator unit, a dosimetry room and an administrative set-up. The treatment room containing the linear accelerator is used for external beam radiation treatment for all types of cancers. The LINAC machine was installed at Sweden Ghana Medical Centre (SGMC) by a Swedish company called Elekta in 2011.

This synergy platform at Sweden Ghana Medical Centre has both photon energy and electron energy. The photon energies produced are 6 MV, and 15 MV while electron energies produced by the machine consist of 6 MeV, 10 MeV and 15 MeV. The machine has a specialized multi-leaf collimator 2 x 40 leafs and 1 cm leaf width at

isocentre. A 30 x 40 cm wedge installed in the synergy platform permits a 40 cm maximum filed size at isocentre. It also has a motorized 60 degree wedge.

In treatment delivery, the LINAC can be used to give three (3) dimensional radiotherapy, intensity modulated radiotherapy (IMRT), volumetric-modulated arc therapy (VMAT), stereotactic radiosurgery (SRS). The treatment couch used at Sweden Ghana Medical Centre is the precise and hexapod type. Plate 3.1 shows Pictorial view of the Synergy Platform Linear Accelerator unit at SGMC.

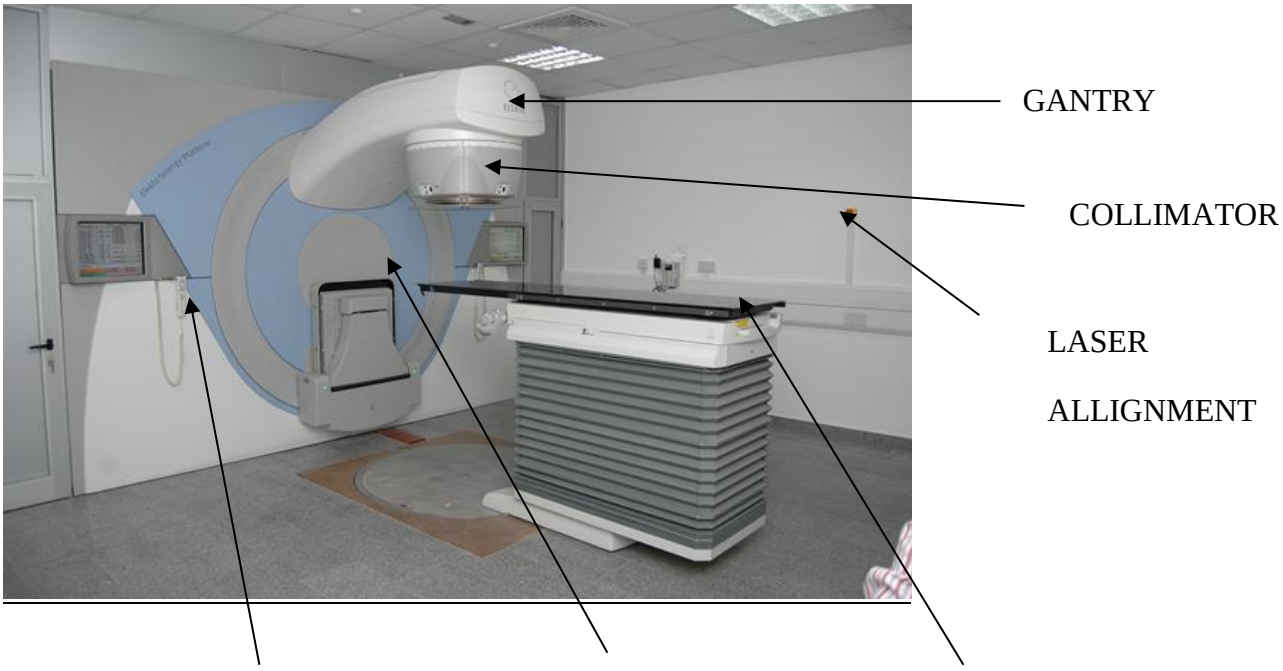

HAND CONTROL BOTTOM GANTRY ANGLE COUCH

Plate 3.1 A Pictorial view of the Synergy Platform Linear Accelerator unit at SGMC

3.1.2 The Motorized Water Phantom used

The type of motorized water phantom used in this study to acquired my data is the Blue water Phantom [2] manufactured by IBA. It consists of a high precise, servo-mechanism for driving the measuring device (ionization chamber) and Perspex water tank of dimension 10 mm side wall thickness and 15 mm base thickness. The dimensions of the water tank is 48 cm x 48 cm x 48 cm. The phantom weighs 45 Kg in the absence of water. The blue phantom and its accessories is a measuring device, for the measurement and analysis of the radiation field of medical linear accelerator [Wellhofer, 2001]. This water phantom forms part of the Omnipro-Accept system. The phantom consists of three-dimensional servo tank, a control unit with integrated two channel electrometer (CCU) and two single detectors (ionization chamber), one for measurement and the other used for reference. Plate 3.2 shows a pictorial view of the blue water phatom[2]

Attached to the phantom to complete the system are tissue maximum ratio set probe (TMR Probe), a separate water reservoir (Plate 3.4), temperature and pressure sensor and a lift table. The tissue maximum ratio (TMR) probe is built with high accurate magnetostrictive positioning technology to accurately measure the changing water level. The water reservoir on a wheel has a pump for uni-directional or bi-directional

water transport to and from the water phantom. It incorporates an electronic pump control system for tissue maximum ratio (TMR) or tissue phantom ratio (TPR) measurement option.

The lift table is used to support and lift the water phantom. It has both manual and electronic (telescope) lifting mechanism for the positioning of the water phantom. The carriage has two fixed and two steerable rollers with brakes, as well as one compartment and two drawers for storing other accessories. Plate 3.3 shows a pictorial view of the electrical lift table for the blue phantom[2].

It is also equipped with a levelling frame for fine adjustment in vertical and horizontal direction. The temperature and pressure sensor is set up inside the water tank for the measurement of water temperature within ± 0.30 ^{o}C. The water temperature measurement is used in combination with the pressure measurement (build-in pressure sensor provided in the CCU) to allow automatic temperature and pressure correction

(KTP) for output factor determination or absolute dosimetry [IBA.,2014]

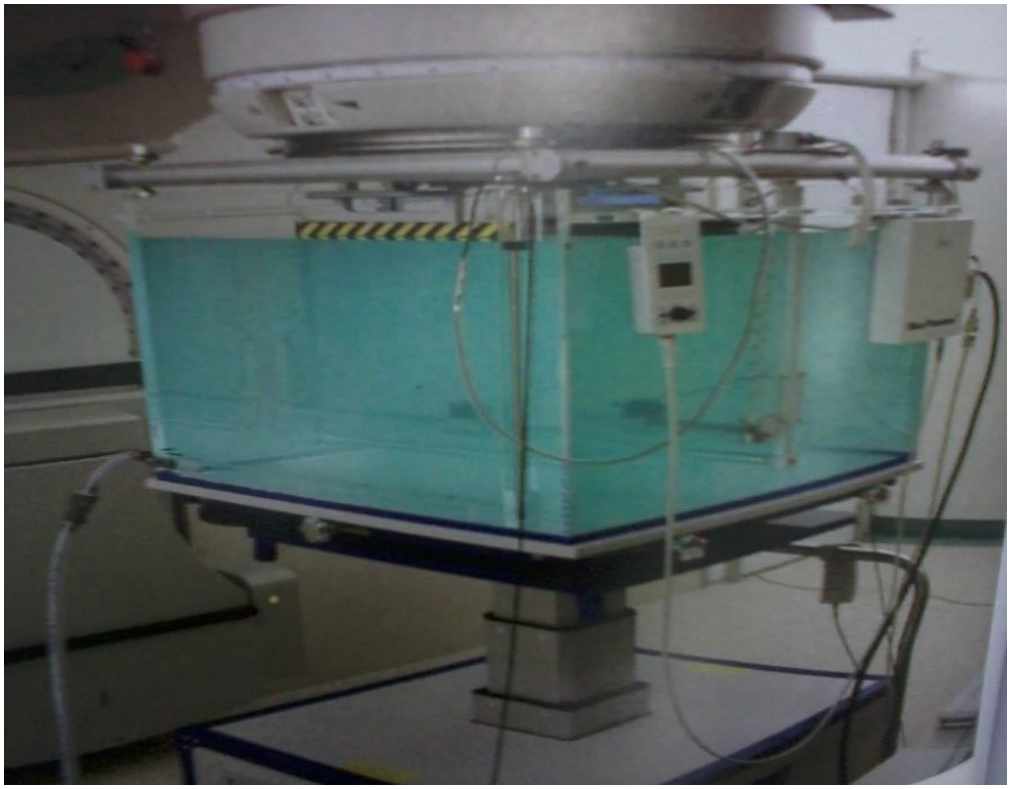

Plate 3.2 A Pictorial view of the blue water phatom[2]

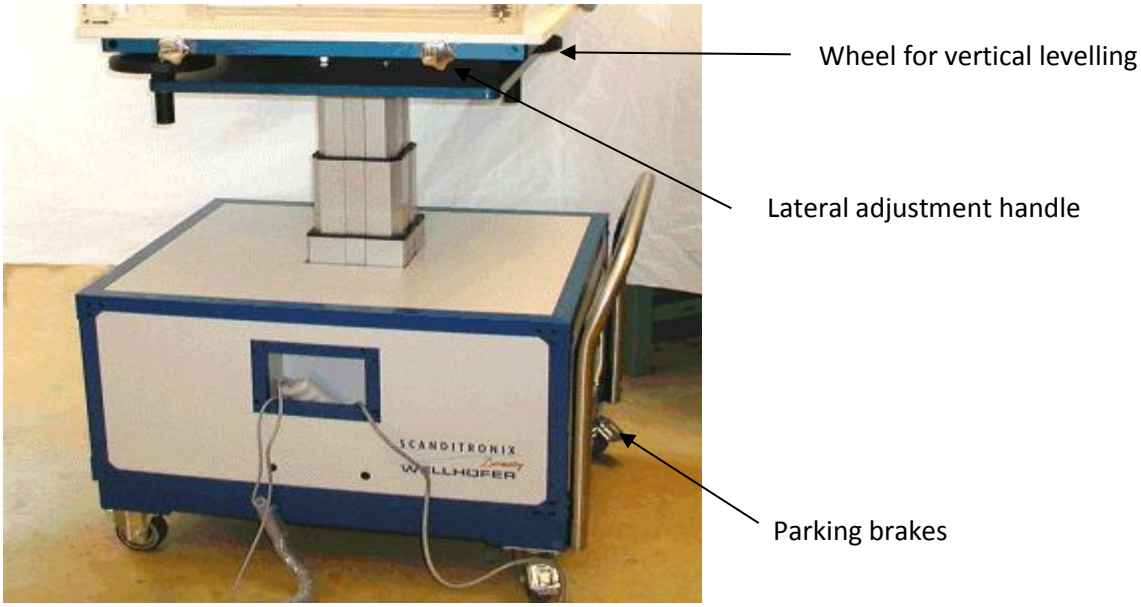

Plate 3.3 A pictorial view of the electrical lift table for the blue phantom[2]

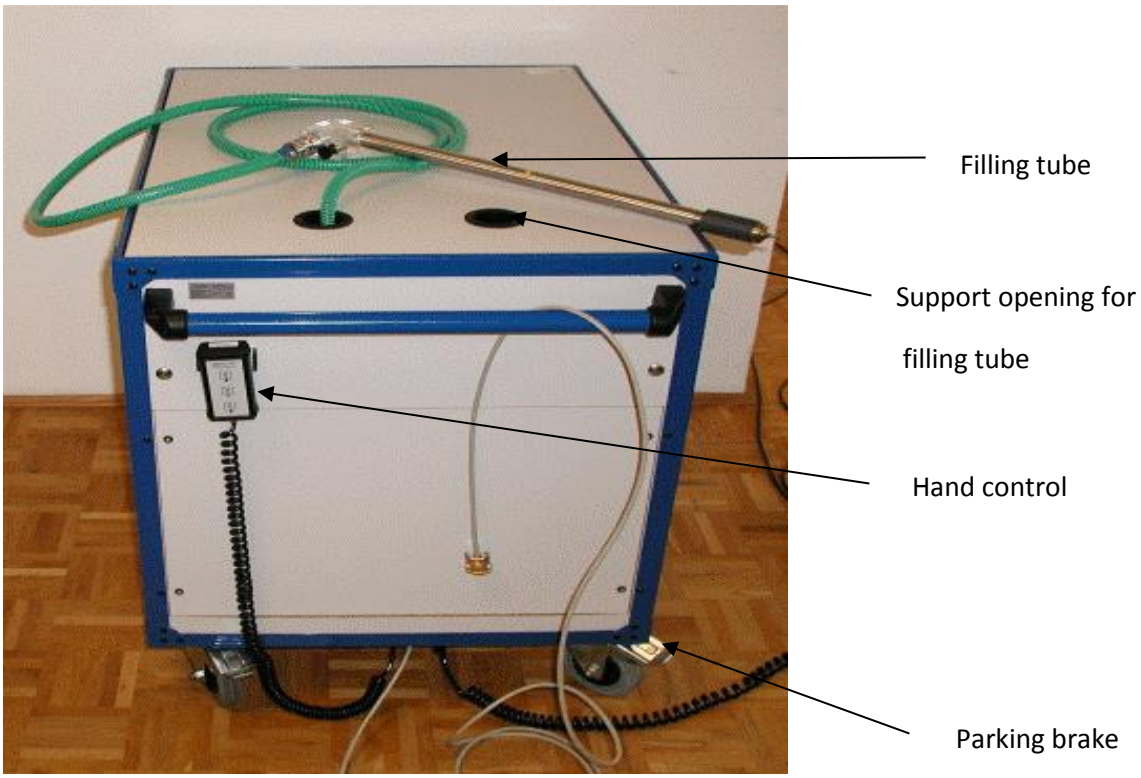

Plate 3.4 A pictorial view of the water reservoir for the blue phantom[2]

3.1.3 The Ionization Chamber used

The type of ionization chamber used at Sweden Ghana Medical Centre (SGMC) for this work was CC13. This type of ionization chamber (CC13) is intended for absolute and relative dosimetry of photon and electron beams in radiotherapy [Gersh, 2014]. PTW Freiburg, Germany (model TNC 0503-00, serial number of 11026), is used. The ionization chamber used was calibrated against a source of known beam quality at the IAEA Secondary Standard Dosimetry Laboratory (SSDL). The calibration was done with a bias voltage of 400 V at the temperature of 293 K (20 ^{0}C), pressure of 101.325

kPa and humidity of 50 %. Measurements can be performed in air, water phantoms or solid phantoms. The CC13 is an air ionization chamber vented through a waterproof silicon sleeve. It is waterproof and fully guarded and is designed for axial or lateral beam entrance. It is used for the measurement of dose rate, absorbed dose to water, air kerma or exposure for radiation therapy calibration measurements in air or solid phantom [IBA, 2013]. Figure 3.1 shows the dimensional specifications of the CC13 ionization chamber.

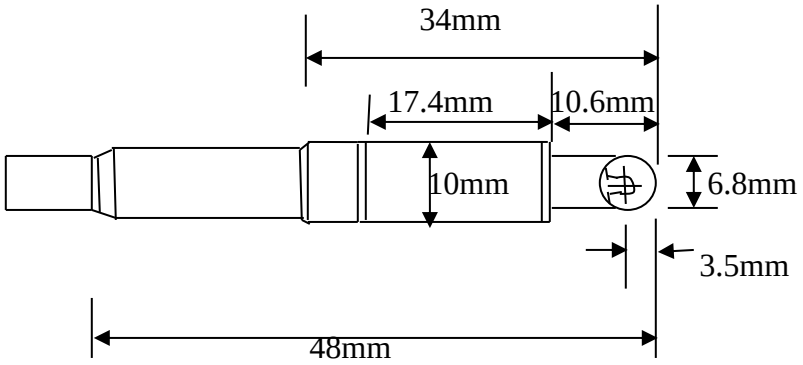

Figure 3.1 dimensional specifications of the CC13 ionization chamber.

The chamber is used only with a dosimeter that meets IEC 60731 requirements and is designed with the same chamber connection as used by IBA Dosimetry. The chamber is therefore not connected to an electrometer designed for grounded input. The detector has a cable length of 1.4 m. Table 3.1 shows the dimensional specifications of the CC13 Ionization Chamber and plate 3.5 shows a pictorial view of the CC13 Ionization Chamber.

Table 3.1: Dimensional specifications of the CC13 Ionization Chamber

Outer dimension	
Part	**Dimension**
Outer chamber diameter	6.8 mm
Chamber stem diameter	10 mm
Build-up cap diameter	9 mm
Stem length	17.4 mm
Total length	48 mm
Inner dimension	
Active volume (nominal)	0.13 cm^3
Total active length	5.8 mm
Cylinder length	2.8 mm
Inner diameter of cylinder	6.0 mm
Wall thickness	0.4 mm
Diameter of inner electrode	1.00 mm
Length of inner electrode	3.3 mm

Plate 3.5 A pictorial view of the CC13 Ionization Chamber.

3.1.4 The Electrometer used

The type of electrometer at SGMC used for this study was a solid state electrometer called the PTW unidos E electrometer. It is an electrometer mainly used for daily routine dosimetry in radiation therapy. Ionization chambers and solid-state detectors can be connected. The chamber library makes it possible to store calibration data. This electrometer displaces measured values of dose and dose rate in Gy, R, Gy/min, R/min or Gy.m. The electrical values of charge and current are measured in coulombs (C) and ampere (A) respectively. The device has high contrast LC display which makes it

easy for measured values to be read. Unidos E electrometer automatically check if there is high voltage between the electrodes of the ionization chamber so as to prevent damage to the ionization chamber.

The electrometer can be operated on both mains and battery power supply. Air density corrections are performed by keying-in air pressure and temperature or by means of a radioactive check device. The check device data are stored in a data babe. This electrometer has automatic noise suppression and automatic built-in system test. It is suitable for high precision dosimetry acceptance test of x-ray equipment using ionization chamber. It is very accurate, having long-term stability, excellent resolution and wide dynamic measuring ranges. It is suitable as a reference class dosimeter according to IEC 60731 for radiation therapy and as in-vivo dosimeter according to IEC 60601-2-9 for patient's dose measurement. Plate 3.6 shows a pictorial view of the PTW Unidos E Electrometer.

Plate 3.6 A pictorial view of the PTW Unidos E Electrometer.

3.1.5 The Distilled Water

About 40 litters of distilled water was used to fill the blue phantom reservoir. Distilled water was used for this experiment because it is uniform and pure whiles undistilled water may contain many different materials in varying concentrations.

Tap water as such, contains various types of natural but relatively harmless contaminants such as scaling agents like calcium carbonate in hard water and metal ions such as magnesium and iron, and odoriferous gases such as hydrogen sulfide. So it is not suitable for this type of research.

3.2 Experimental Method

In this experiment, percentage depth dose (PDD) values and tissue maximum ratio (TMR) values were measured at field sizes 5x5 cm, 7x7 cm, 8x8 cm, 10x10 cm, 12x12 cm, 15x15 cm, 20x20 cm, 25x25 cm, 30x30 cm and 40x40 cm and depth from 1.5 cm, 2 cm, 3 cm, 4 cm to 25 cm for 6 MV and 15 MV x-ray beam.

3.2.1 Measurement of Percentage Depth Dose (PDD)

In this measurement, the motorized water phantom was placed on the lift table and the set up was left under the gantry. The distilled water was pumped into the tank of the phantom until it reached the required mark on the phantom. Though there is a built-in temperature and pressure correction in the phantom, the set up was still left in the room overnight so that the water could be adjusted to the room temperature. The distance from the source to the surface of the water in the phantom (SSD) was

adjusted by the help of the remote control to 100 cm. The tissue maximum ratio (TMR) set probe was deactivated from the motorized water phantom. The levelling frame with a cross mark on it is moved on the water surface in all directions so that the midpoint of the cross mark coincides with the water surface, to ensure fine adjustment in vertical and horizontal leveling of the water in the tank. By the help of the lasers in the treatment room, the CC13 ionization chamber was fixed into the water phantom such that the sensitive part coincides with the cross point of the laser on the water surface (that is; 100 cm SSD). All other connections including the cable from the CC13 ionization chamber to the PTW unidos E electrometer were ensured to be tightly fixed. The central axis was defined. This causes the ionization chamber to move through the water phantom along the central axis. A scan length of 1 cm and all necessary parameters for the field including the field size were entered in the basic setting area. This permits the dose to be recorded after every 1 cm depth of travel of the ionization chamber along the same central axis. By selecting common setting, then choosing on calculation option and finally selecting depth dose calculation on the Omnipro-Accept software, the percentage depth dose values were measured for 6 MV and 15 MV.

3.2.2 Measurement of Tissue Maximum Ratio (TMR)

The blue phantom[2] was placed on the lift table and they were positioned under the gantry. The z axis of the motorized water phantom was deactivated and the TMR probe activated instead. The pump from the reservoir was connected to the water phantom and the software Omnipro-Accept was used to switch on and off the pump

when required. To ensure that other measurements other than TMR would not affect the TMR measurement, the phantom (tank) was first emptied and was filled with the distilled water so that about 15 cm of water remained in it. This initial 15 cm of distilled water in the tank was needed to provide correct backscatter condition. The phantom was lifted up with the lift table so that the LINAC's isocentre (cross point of lasers) matched the actual water surface. The float which runs up and down on the linear transducer was also allowed to sit on the water surface too. Using the hand control, the isocentre and water surface were redefined at the same point where the chamber was sitting in the linac's isocentre, which matches the actual surface. With this set up, the first measurement started at the isocentre after performing the 2 cm empty/refill procedure to stabilize the water surface [Das et al., 2008]. A scan length of 1 cm and all other parameters of the field including field size were entered in the basic setting area. With the Omnipro-Accept software, the tissue maximum ratio (TMR) values were measured for 6 MV open field and 15 MV open field. Plate 3.7 shows a pictorial view of the set-up for measuring TMR when the phantom was filled with 10 cm of distilled water and Plate 3.8 shows a pictorial view of the set-up for measuring TMR when the phantom was fully filled with distilled water.

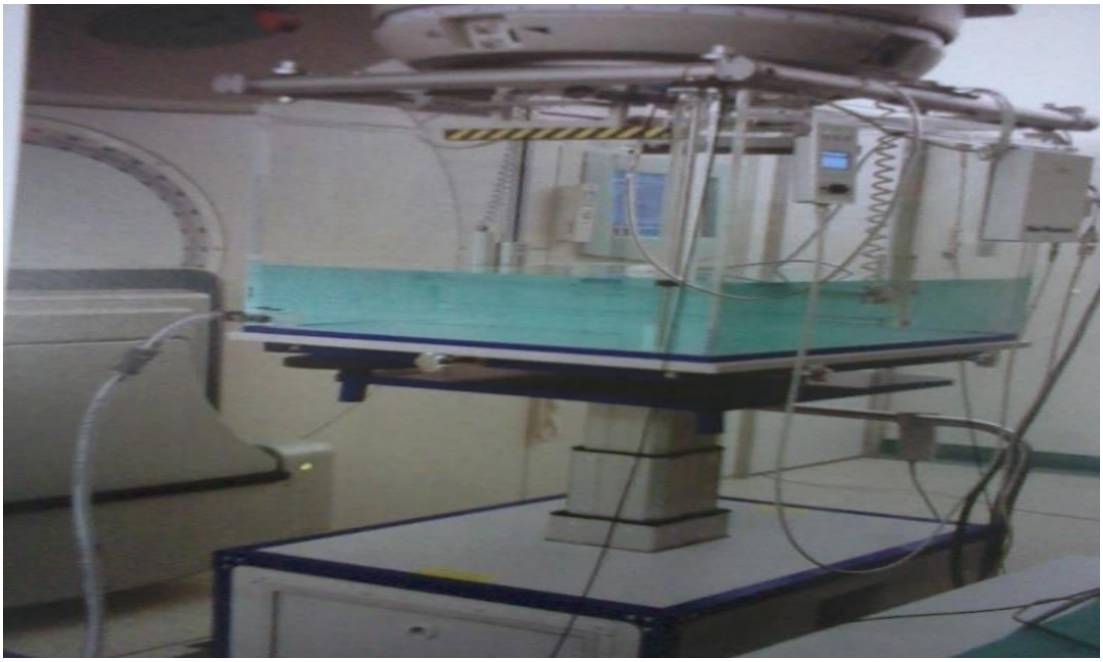

Plate 3.7 A pictorial view of the set-up for measuring TMR when the phantom was filled with 10 cm of distilled water

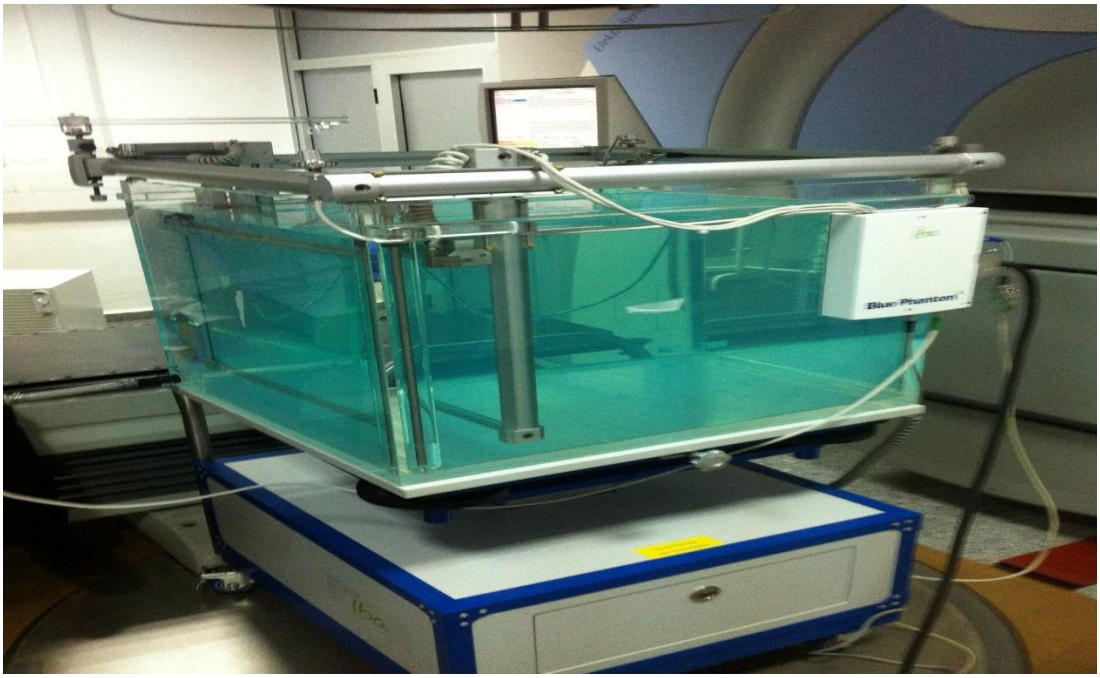

Plate 3.8 A pictorial view of the set-up for measuring TMR when the phantom was fully filled with distilled water

3.3 Determination of Phantom Scatter Factors (S_p)

Phantom scatter factor could not be measured directly. In the determination of this factor, total scatter factor (S_{cp}) and the collimator scatter factor (S_c) were measured.

For the determination of the total scatter factor (S_{cp}), the ionization chamber was positioned at d_{max} in the water phantom and distilled water was pumped into the phantom to the required mark. It was ensured that, the depth of water beyond d_{max} down to the bottom was at least 10 cm so as to provide full back scatter. The field size of interest was set from the collimator setting. The SSD was set to 100 cm and the detector positioned at the isocentre. A scan was made and the dose at d_{max} was recorded. The procedure was repeated with the same monitor unit and the detector still at $d_{max,}$ except that the field size was changed to reference field of 10x10 cm^2. The dose was recorded and the total scatter factor (S_{cp}) was then calculated from equation 2.8 of section 2.7.1

In the determination of the collimator scatter factor (in-air output), the SSD was set to 100 cm. Large build up caps in brass with a wall thickness of 2.4 mm at 6 MV and 8 mm at 15 MV were used on the ionization chamber so as to prevent the chamber from measuring contaminated electrons in the beam. The set up was left in air. The collimator was opened to an arbitrary value and the scan was made to record the charge collision in air. With the same monitor unit, reference SSD (100 cm) and build up cap on ionization chamber, the kerma in air was again determined when the collimator setting was at the reference size of 10x10 cm^2. The collimator scatter factor (S_c) was determined using equation 2.9 of section 2.7.1

After both S_{cp} and S_c were obtained, the phantom scatter factor (S_p) was calculated using equation 2.7 of section 2.7.1

3.4 Determination of Doses from the Treatment Planning System (TPS) and Tissue Maximum Ratio (TMR)

The type of TPS use at SGMC for the study is the Oncentra MasterPlan version 4.3. By the use of this TPS, 40x40x40 cm^3 phantom is created in the masterPlan. Doses at field sizes 4x4 cm, 10x10 cm, 25x25 cm, 30x30 cm and 40x40 cm were obtained from the treatment planning system (Oncentra MasterPlan) for the energies, 6 MV and 15 MV. These doses were found at isocentre for each field size and depth. For these field sizes and depths, the doses for the two energy beams were calculated manually, using the measured and the calculated TMR values, by the help of equation 2.10 of section 2.8. The calibration factor (CF) used for the linac at SGMC is 0.01 Gy/min

The calculated doses at isocentre from both the measured and calculated TMRs were then compared with those obtained during commission from the MasterPlan TPS and the percentage deviations were obtained.

CHAPTER FOUR

RESULTS AND DISCUSSION

This chapter focuses on the percentage depth dose data (PDD) and tissue maximum ratio data (TMR) measured in a period of one month at Sweden Ghana Medical Centre (SGMC), and results of calculated TMR data obtained using equation 2.6 of section 2.7 of chapter two.

4.1 Data for discussion and analysis

Selected square field sizes of; 5x5, 7x7, 10x10, 12x12, 15x15, 20x20, 25x25, 30x30 and 40x40 cm^2 were taken for data analysis and discussion. For the analysis and discussion, the depth of measurement will be restricted to 1.5 cm, 2 cm, 2.5 cm, 2.6 cm, 3 cm, 4 cm, 6 cm, 8 cm, 10 cm, 12 cm, 14 cm, 16cm, 18 cm, 20cm, 22 cm and 24 cm. Measured PPD data for 6 MV and 15 MV are presented in table 4.1 and table 4.2 respectively. Measured TMR data for 6 MV and 15 MV are presented in table 4.3 and 4.4 respectively. The calculated TMRs for 6 MV and 15 MV at various field sizes and depths are respectively listed in tables 4.5 and 4.6. Figures 4.1 and 4.2 show plots of percentage depth dose as a function of depth for the two different energies at field sizes 5x5 cm and 10x10 cm respective. The variations of tissue maximum ratios (TMRs) as a function of depth and energy are depicted in figure 4.3 and 4.2 respectively. Figure 4.5 shows how the measured TMR for 15 MV varies with field size whiles the variations of PDD at 15 MV with field sizes are demonstrated in figure 4.6. Plots showing how the measured and the calculated TMRs vary with depth at 5x5

cm and 40x40 cm for 6 MV are presented in figure 4.7 and figure 4.8 respectively. Figures 4.9 and 4.10 also depict how the measured and the calculated TMRs varies with depth at 5x5 cm and 40x40 cm for 6 MV and 15 MV respectively. The determined relative differences between the measured and the calculated TMRs for 6 MV and 15 MV are presented in figures 4.11 and 4.12 respectively. The percentage deviations of both the measured and the calculated TMRs from that on the treatment planning system at various field sizes are shown in figure 4.13 an figure 4.14 for 6 MV and 15 MV respectively.

4.1.1 Measured Percentage Depth Dose (PDD) Data

Table 4.1 Measured percentage depth dose (PDD) for 6 MV open field

	square field size (cm^2)								
depth(cm)	**5x5**	**7x7**	**10x10**	**12x12**	**15x15**	**20x20**	**25x25**	**30x30**	**40x40**
1.5	100.0	100.0	100.0	100.0	100.0	100.0	100.0	100.0	100.0
2.0	99.6	99.6	99.4	99.4	99.2	99.1	99.0	98.9	98.9
3.0	95.2	95.5	95.7	95.5	95.5	95.5	95.4	95.4	95.8
4.0	90.5	91.0	91.4	91.5	91.6	91.9	91.7	92.0	92.3
6.0	81.3	82.3	83.2	83.6	84.0	84.4	84.6	84.9	85.5
8.0	72.7	74.0	75.3	76.0	76.6	77.4	77.8	78.3	78.9
10.0	64.8	66.3	68.0	68.9	69.7	70.6	71.3	71.8	72.6
12.0	57.6	59.3	61.2	62.2	63.2	64.4	65.2	65.8	66.8
14.0	51.2	53.1	55.1	56.1	57.3	58.5	59.4	60.2	61.3
16.0	45.7	47.5	49.5	50.5	51.8	53.1	54.3	55.0	56.2
18.0	40.6	42.4	44.4	45.5	46.7	48.4	49.3	50.2	51.4
20.0	36.3	38.0	39.8	40.9	42.2	43.8	44.9	45.8	47.0
22.0	32.3	33.9	35.8	36.9	38.1	39.7	40.9	41.7	43.0
24.0	28.9	30.3	32.2	33.2	34.4	36.0	37.1	38.0	39.2

From the measured PDD data for 6 MV shown in the table above, there is a decrease in PDD with depth for all field sizes. The depth of maximum dose (d_{max}) occurred at 1.5 cm. It is observed that for the 6 MV megavoltage beam, the PDD values at a

depths just below d_{max} decrease with increasing field size after which, at all other depths below d_{max}, PDD values increase with increasing field size. The rate of increase of PDD with field size is high at deeper depth as compared to those at shallow depth

Table 4.2 Measured percentage depth dose (PDD) for 15 MV open field

	Square field size (cm^2)								
Depth (cm)	**5x5**	**7x7**	**10x10**	**12x12**	**15x15**	**20x20**	**25x25**	**30x30**	**40x40**
2.6	100.0	100.0	100.0	100.0	100.0	100.0	100.0	100.0	100.0
3.0	99.8	100.0	99.8	99.5	99.3	99.2	99.2	99.2	99.2
4.0	97.3	97.4	97.1	96.6	96.6	96.3	96.3	96.1	96.4
6.0	89.5	89.8	89.8	89.5	89.6	89.5	89.6	89.6	90.1
8.0	81.5	82.4	82.6	82.7	82.9	82.9	83.2	83.4	83.9
10.0	74.4	75.3	75.9	76.0	76.5	76.8	77.2	77.4	78.1
12.0	67.7	68.8	69.6	69.9	70.4	70.8	71.5	71.8	72.5
14.0	61.7	62.9	63.9	64.2	64.9	65.5	66.0	66.6	67.3
16.0	56.2	57.3	58.4	58.9	59.6	60.4	61.1	61.7	62.5
18.0	51.0	52.4	53.6	54.0	54.8	55.7	56.5	57.0	58.0
20.0	46.6	47.9	49.0	49.6	50.4	51.4	52.1	52.7	53.7
22.0	42.5	43.7	45.0	45.6	46.5	47.3	48.1	48.8	49.8
24.0	38.8	39.9	41.2	41.8	42.7	43.7	44.5	45.1	46.1

From table 4.2 above, similar occurrences in table 4.1 are observed except that the depth of maximum dose (d_{max}) for the 15 MV megavoltage beam in table 4.2 occurred at a depth of 2.6 cm which is deeper than that of 6 MV in table 4.1

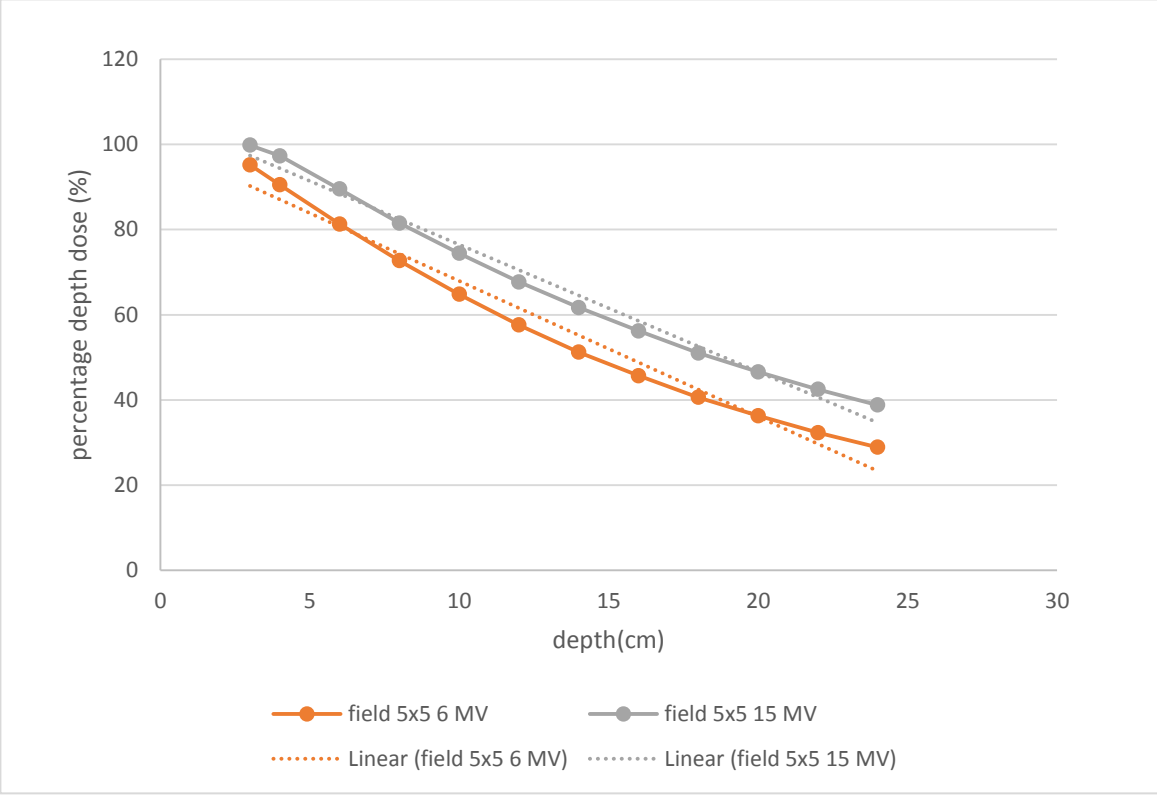

Figure 4.1: A graph of pdd (%) against depth (cm) for 6 MV and 15 MV at 5x5 field size

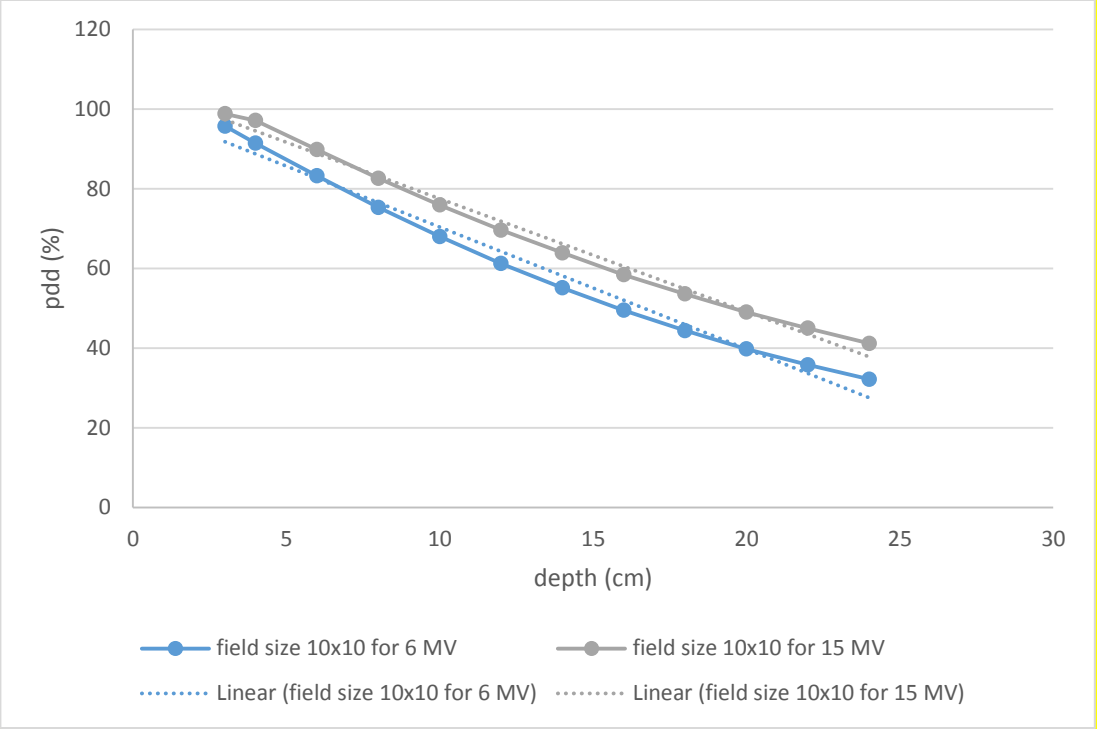

Figure 4.2: A graph of pdd (%) against depth (cm) for 6 MV and 15 MV at 10x10 field size

4.1.1.1 Dependence of Percentage Depth Dose (PDD) on Energy of the Photon

From figure 4.1 and figure 4.2 above, as the energy increases from 6 MV to 15 MV, the PDD value also increases. This is due to the effect of secondary electrons produced by the high megavoltage beam. When the energy was increased to 15 MV, the scattered radiations produced by this high megavoltage beam are moved in the forward direction. Thus any electron ejected by the scattered photons are caused to move down in the medium with a high range to increase dose at every depth. But for the low megavoltage beam, the scattered radiations produce move laterally to the primary beam path and hence the resulting secondary electrons produced have short range and cannot travel deep through the medium to increase depth dose. Again, the

difference in percentage dose between these two energies is seen from the two graphs to be significant at higher depths, because slow moving electrons produced by low megavoltage beams cannot travel to a deeper depth to deposit dose as compared with high speed electrons produced by high megavoltage beam.

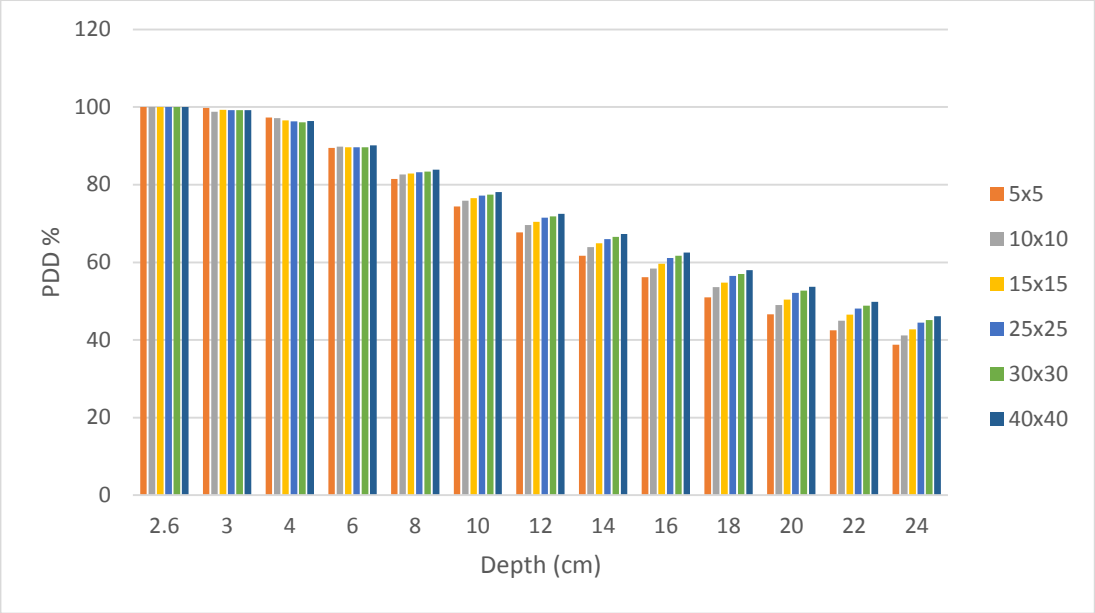

Figure 4.3: A graph of PDD against depth (cm) for 15 MV at different field sizes

The bar graph in figure 4.3 above shows how PPD varies with field size as the depth in the medium becomes deeper. From figure 4.3, the increase in PDD with field size becomes more pronounce at deeper depths.

4.1.2 Measured Tissue Maximum Ratio (TMR) Data

Table 4.3 Measured tissue maximum ratio (TMR) for 6 MV open field

	Square field size (cm^2)								
depth (cm)	**5x5**	**7x7**	**10x10**	**12x12**	**15x15**	**20x20**	**25x25**	**30x30**	**40x40**
1.5	1.000	1.000	1.000	1.000	1.000	1.000	1.000	1.000	1.000
2.0	1.005	1.004	1.002	1.002	1.000	0.999	1.000	0.999	0.998
3.0	0.979	0.981	0.984	0.982	0.982	0.982	0.982	0.982	0.985
4.0	0.947	0.952	0.958	0.959	0.960	0.962	0.963	0.964	0.967
6.0	0.882	0.893	0.905	0.908	0.912	0.916	0.920	0.923	0.929
8.0	0.816	0.830	0.846	0.854	0.861	0.870	0.876	0.882	0.889
10.0	0.753	0.770	0.790	0.800	0.811	0.822	0.831	0.838	0.848
12.0	0.692	0.711	0.735	0.746	0.760	0.775	0.786	0.794	0.807
14.0	0.635	0.657	0.682	0.694	0.710	0.727	0.740	0.750	0.764
16.0	0.583	0.605	0.632	0.645	0.661	0.679	0.695	0.708	0.723
18.0	0.535	0.558	0.585	0.598	0.615	0.636	0.653	0.665	0.682
20.0	0.492	0.513	0.540	0.552	0.571	0.593	0.612	0.625	0.642
22.0	0.451	0.473	0.499	0.512	0.531	0.553	0.572	0.586	0.605
24.0	0.413	0.436	0.461	0.473	0.492	0.515	0.534	0.549	0.569

From the measured TMR data for 6 MV shown in the table 4.3 above, there is a decrease in TMR with depth for all field sizes. The depth of maximum dose (d_{max})

occurred at 1.5 cm. It is observed that for the 6 MV megavoltage beam, the TMR values at a depths just below d_{max} decrease with increasing field size after which, at all other depths below d_{max}, TMR values increase with increasing field size. The rate of increase of TMR with field size is high at deeper depth as compared with those at shallow depth

Table 4.4 Measured tissue maximum ratio (TMR) for 15 MV open field

	Squared field size (cm^2)								
Depth (cm)	**5x5**	**7x7**	**10x10**	**12x12**	**15x15**	**20x20**	**25x25**	**30x30**	**40x40**
2.5	1.000	1.000	1.000	1.000	1.000	1.000	1.000	1.000	1.000
3.0	1.009	1.012	1.008	1.005	1.002	1.000	1.000	1.000	1.000
4.0	1.002	1.004	1.001	0.995	0.993	0.990	0.989	0.988	0.990
6.0	0.956	0.960	0.959	0.956	0.956	0.955	0.955	0.956	0.959
8.0	0.902	0.913	0.914	0.915	0.916	0.917	0.919	0.922	0.927
10.0	0.853	0.863	0.870	0.872	0.876	0.880	0.884	0.887	0.894
12.0	0.804	0.815	0.826	0.830	0.834	0.839	0.846	0.853	0.859
14.0	0.757	0.771	0.783	0.788	0.794	0.802	0.808	0.815	0.824
16.0	0.710	0.726	0.739	.0746	0.754	0.763	0.772	0.781	0.791
18.0	0.667	0.684	0.699	0.707	0.715	0.727	0.737	0.746	0.757
20.0	0.627	0.644	0.660	0.669	0.678	0.690	0.702	0.711	0.723
22.0	0.590	0.606	0.623	0.630	.643	0.657	0.668	0.678	0.691
24.0	0.555	0.571	0.588	0.598	0.608	0.623	0.636	0.645	0.659

From table 4.4 above, similar behavior in table 4.3 are observed except that the depth of maximum dose (d_{max}) for the 15 MV megavoltage beam in table 4.4 occurred at a depth of 2.5 cm which is deeper than that of 6 MV in table 4.3

4.1.2.1 Tissue Maximum Ratio (TMR) Dependence on Energy

From figures 4.4 and 4.5 below, TMR values for the 15 MV x-rays at all depth were found to be greater than that of 6 MV x-rays. The variation of TMR with energy is like that observed with PDD of section 4.1.1.1.

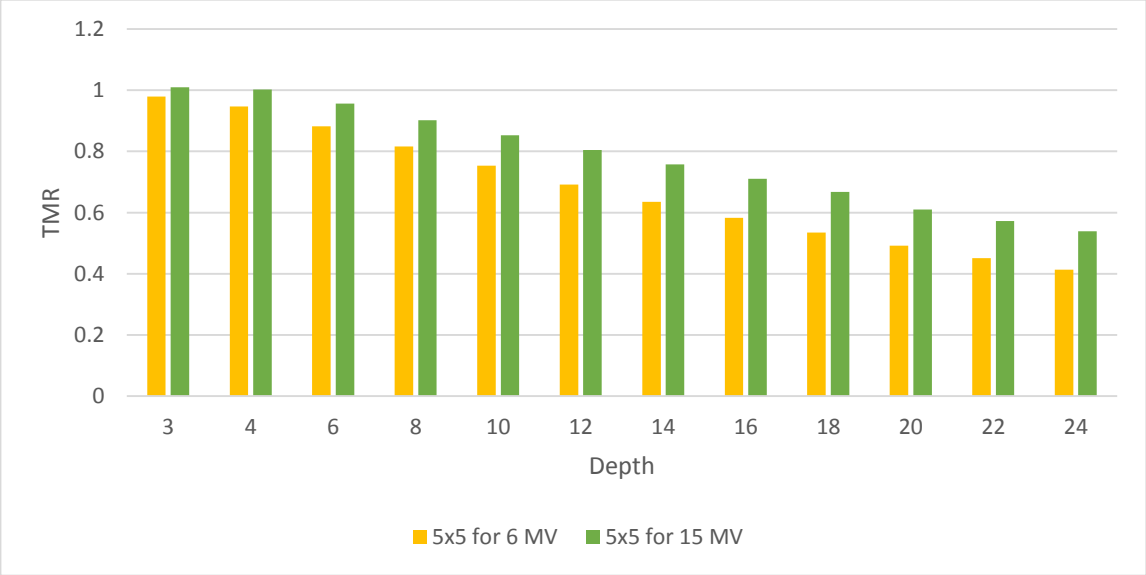

Figure 4.4: A graph of TMR against depth (cm) for 6 MV and 15 MV at 5x5 field size

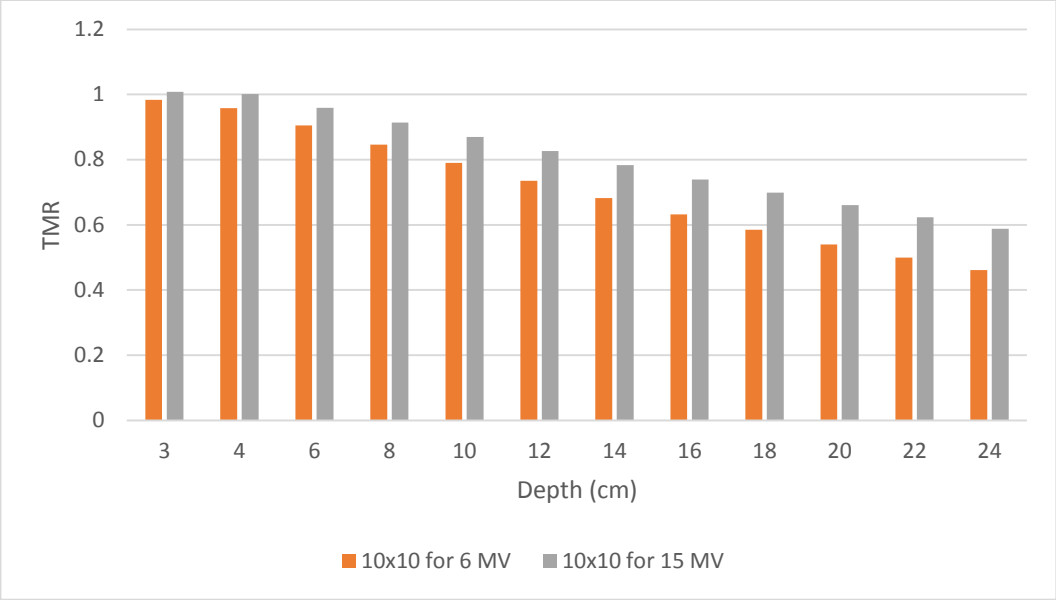

Figure 4.5: A graph of TMR against depth (cm) for 6 MV and 15 MV at 10x10 field size

As explained earlier, the high megavoltage beam produces scattered radiations which move in the forward direction to increase depth dose, thereby increasing tissue maximum ratio. The higher the beam energy, the larger the range of the secondary electrons produced in the forward direction and the higher the TMR. It can be observed from figures 4.4 and 4.5 that the difference in TMR between the two megavoltage beam is significant at deeper depth because the range of the secondary electrons produced by the high megavoltage beam is large and this causes them to travel deeper depth before the shed off all their energies while those produced by the low megavoltage beam travel shorter distance to shed off all of their energies.

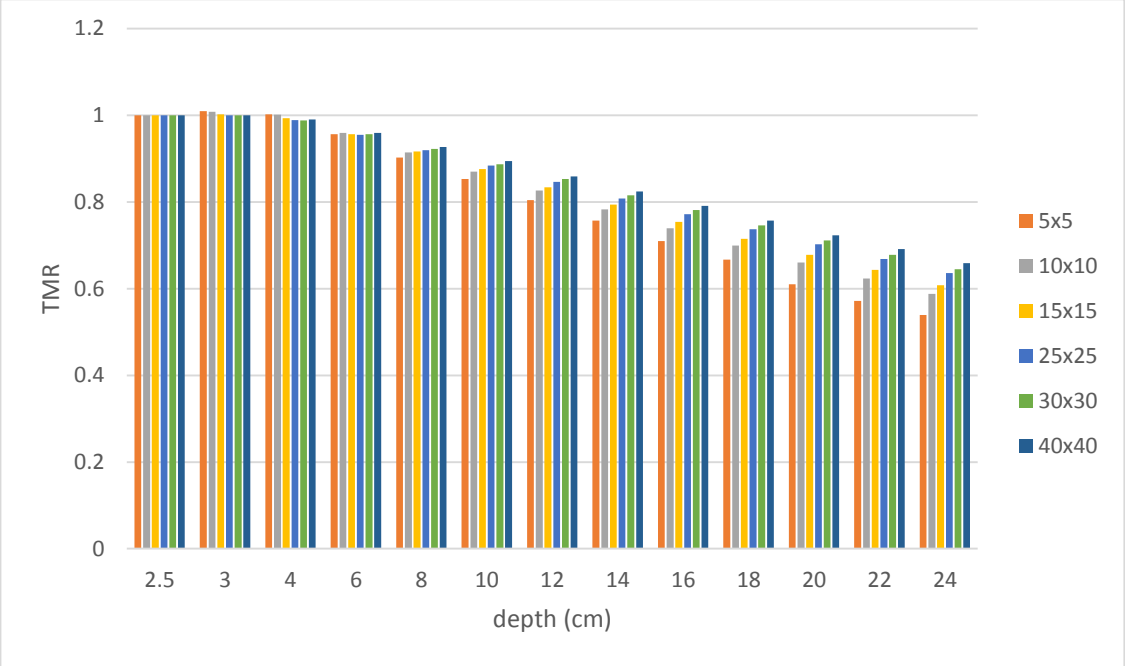

Figure 4.6: A graph of measured TMR against depth (cm) for 15 MV at different field sizes

The bar graph in figure 4.6 above shows how TMR varies with field size as the depth in the medium becomes deeper. From figure 4.6, the increase in TMR with field size becomes more pronounce at deeper depths.

4.1.2.2. Dependence of Depth of Maximum Dose (d_{max}) on Energy.

It can be observed from table 4.1 and 4.3 that, the reference depths (d_{max}) for the 6 MV x-ray beam were close to the surface (that is at 1.5 cm depth) than that of the 15 MV x-ray which were found to be at 2.6 cm and 2.5 cm below the surface of the phantom shown in tables 4.2 and 4.4 respectively. This is because, as high energy photon beam interacts with the medium it imparts either all or part of its energy (as kinetic energy) to the electrons on the surface and as the photon continues to travel deep in the medium more electrons underneath the surface are also set into motion. The range of

these electrons depends on the energy imparted to them but the higher the energy of the photon beam, the greater the energy imparted to the electrons and the longer the range. As the photon beam continues to interact with the medium, more electrons are set into motion and as they travel this maximum range they stop and shed all their energy to the medium till charge particle equilibrium is reached where any photon incident on the medium, does not further produce a moving electron. This maximum point where the electrons stop to shed their energy is called the build-up region and the distance from the surface to this point is called the depth of maximum dose (d_{max}). However, because the range of electrons produced by high megavoltage beam is longer than that produced by low energy photon beam, d_{max} of 15 MV is deeper than that of 6 MV.

4.1.2.3 Variation of tissue maximum ratio (TMR) and percentage depth dose (PDD) with field size

From figures 4.3 and 4.6, it can be observed that, both PDD and TMR values at 2.5 cm depth are the same for all field sizes and this represents the d_{max} for the 15 MV x-ray beam. This continues with a decrease in TMR as field size increases till a depth of 6 cm above which it begins to increase with field size.

This is in contrast with normal expected behavior because TMR increases with field size at all depths above the build-up region. The unexpected decrease in TMR with field size is due to; incident scattered radiation, changing balance with depth of phantom scatter and the presence of secondary electrons from the beam. As clearly

pointed out in BJR supplement 17, an increase in incident scatter radiation with field size causes a reduction in depth dose whiles an equivalent increase in phantom scatter with field size causes an increase in the depth dose. Also contaminated electrons increases with dose to a level of most energetic secondary electron. These three effects balances at some focused depth in such a way that, PDD values are no more field dependent. It is observed again that the change in TMR with field size is very significant at higher depths.

From figures 4.3 and 4.6, the increase in depth dose and TMR is as a result of scattered photons. As field size increases, more scattered photons are produced which eject more secondary electrons to contribute to the depth dose. Because the effect of scattered radiation is more predominant with depth, the increase in TMR and PDD with field size becomes significant with depth.

4.1.2.4: Variation of tissue maximum ratio (TMR) and percentage depth dose (PDD) with depth

Figures 4.3 - 4.6 depict that, at all field sizes above 2.6 cm, both percentage depth dose and tissue maximum ratio decrease with increasing depth (distance) in the phantom for both 6 MV and 15 MV. This is because of attenuation. Since inverse square law is less pronounced in this effect, as the depth in the phantom increases, the progressive loss of energy by the photon beam also increases and as a result produces secondary electrons with short range. This makes the number of secondary electrons reaching deeper depths to be reduced, hence causing a decrease in depth dose and tissue

maximum ratio. As explained earlier in section 4.1.2.2, after charge particle equilibrium (which ocurrs at d_{max}), where no further electron is set into motion, the energy imparted to the medium by the electron as a dose also starts to decline. Thus the decrease in PDD and TMR started after d_{max}. As pointed out by Leon et al., 1993 that attenuation is inevitable so far as photon interacts with a medium, there is always variation in depth dose with depth in a phantom

4.1.3 Calculated TMR Data

Some selected field sizes of 5x5, 7x7, 10x10, 12x12, 15x15, 20x20, 25x25, 30x30 and 40x40 and depths of 1.5 cm, 2 cm, 4 cm, 6cm, 8 cm, 12 cm, 14 cm, 16 cm, 18 cm, 20 cm, 22 cm, and 24 cm were used to calculate for the tissue maximum ratio (TMR) values from the percentage depth dose data.

Table 4.5: Calculated tissue maximum ratio (TMR) for 6 MV open field

	Square field size (cm^2)								
Depth(cm)	5x5	7x7	10x10	12x12	15x15	20x20	25x25	30x30	40x40
1.5	1.000	1.000	1.000	1.000	1.000	1.000	1.000	1.000	1.000
2.0	1.006	1.006	1.004	1.004	1.002	1.001	1.000	0.999	0.999
3.0	0.980	0.983	0.985	0.983	0.983	0.983	0.982	0.982	0.987
4.0	0.950	0.955	0.960	0.961	0.962	0.965	0.963	0.966	0.969
6.0	0.887	0.898	0.907	0.912	0.916	0.920	0.923	0.926	0.932
8.0	0.823	0.838	0.853	0.860	0.867	0.876	0.881	0.886	0.893
10.0	0.761	0.779	0.799	0.809	0.819	0.829	0.837	0.843	0.853
12.0	0.701	0.722	0.745	0.757	0.770	0.784	0.794	0.801	0.813

14.0	0.646	0.670	0.695	0.708	0.723	0.738	0.749	0.759	0.773
16.0	0.597	0.620	0.647	0.660	0.677	0.694	0.709	0.7184	0.734
18.0	0.549	0.573	0.600	0.615	0.631	0.654	0.666	0.678	0.695
20.0	0.507	0.531	0.556	0.572	0.590	0.612	0.628	0.640	0.657
22.0	0.467	0.490	0.517	0.533	0.550	0.574	0.591	0.602	0.621
24.0	0.431	0.452	0.481	0.496	0.513	0.537	0.553	0.567	0.585

From table 4.5, the calculated TMR has the depth of maximum dose (d_{max}) at 1.5 cm. The TMR values, decrease with depth but increase with field size except the depth (2 cm) just below d_{max} which shows a decrease in TMR with field size. The increase in TMR with field size is significant at higher depths.

Table 4.6: Calculated tissue maximum ratio (TMR) for 15 MV open field

	Square field size (cm^2)								
depth	5x5	7x7	10x10	12x12	15x15	20x20	25x25	30x30	40x40
2.6	1.000	1.000	1.000	1.000	1.000	1.000	1.000	1.000	1.000
3.0	1.006	1.008	1.006	1.002	1.001	1.000	1.000	1.000	1.000
4.0	1.000	1.001	0.998	0.993	0.993	0.989	0.989	0.987	0.990
6.0	0.955	0.959	0.959	0.955	0.956	0.955	0.956	0.956	0.962
8.0	0.903	0.913	0.915	0.916	0.919	0.919	0.922	0.924	0.930
10.0	0.855	0.866	0.872	0.874	0.879	0.883	0.887	0.890	0.898
12.0	0.807	0.820	0.829	0.833	0.839	0.844	0.852	0.856	0.864
14.0	0.762	0.777	0.789	0.793	0.801	0.809	0.815	0.822	0.831
16.0	0.718	0.732	0.747	0.753	0.762	0.772	0.781	0.789	0.799
18.0	0.675	0.693	0.709	0.714	0.725	0.737	0.747	0.754	0.767
20.0	0.637	0.655	0.670	0.678	0.689	0.703	0.713	0.721	0.735
22.0	0.601	0.618	0.636	0.645	0.657	0.669	0.680	0.690	0.704
24.0	0.567	0.583	0.602	0.611	0.624	0.638	0.650	0.659	0.673

Table 4.6 also depicts similar behavior as found in table 4.5, except that the depth of maximum dose (d_{max}) occurred at 2.6 cm which is higher than that found with the 6 MV megavoltage beam in table 4.5.

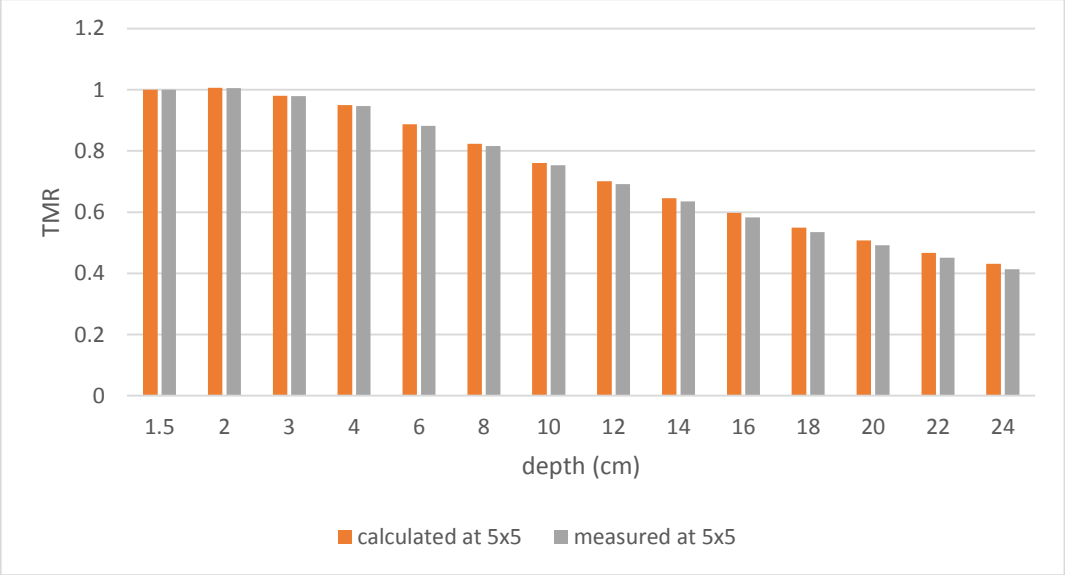

Figure 4.7: A graph of calculated and measured TMR against depth (cm) for 6 MV at 5x5 field sizes.

From figure 4.7, both the calculated and the measured TMRs at field size 5x5cm vary in inverse proportion with depth in the phantom above 2 cm depth. From the depth of 1.5 cm to 12 cm, there was good agreement between the calculated and the measured TMR but they started to disagree after 12 cm depth where the calculated TMR values exceeded the measured values. This calls for consideration of calculated TMR values used in treatment time calculation when treating a deep tumor.

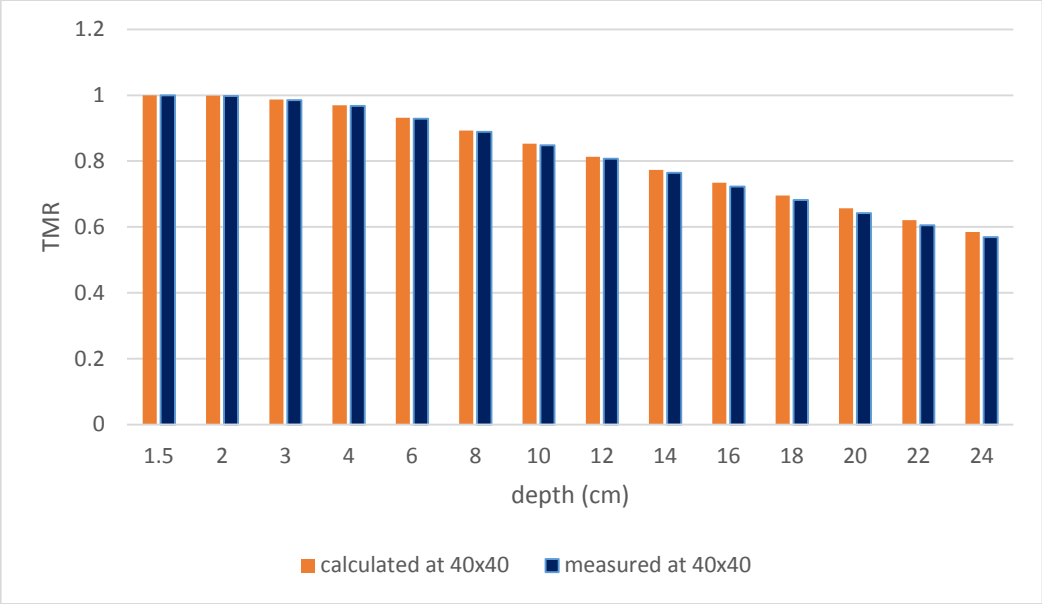

Figure 4.8: A graph of calculated and measured TMR against depth (cm) for 6 MV at 40x40 field sizes

Figure 4.8 depicts the fact that at the same depth and energy, the calculated TMR agrees well with the measured TMR for 40x40 cm field size as compared with that at 5x5 cm. Again from figure 4.8, there is a good correlation between the calculated TMR values and their measured counterpart from the depth of 1.5 cm to 16 cm after which they started to show small deviation, where the calculated TMR values became greater than that of the measured TMR values.

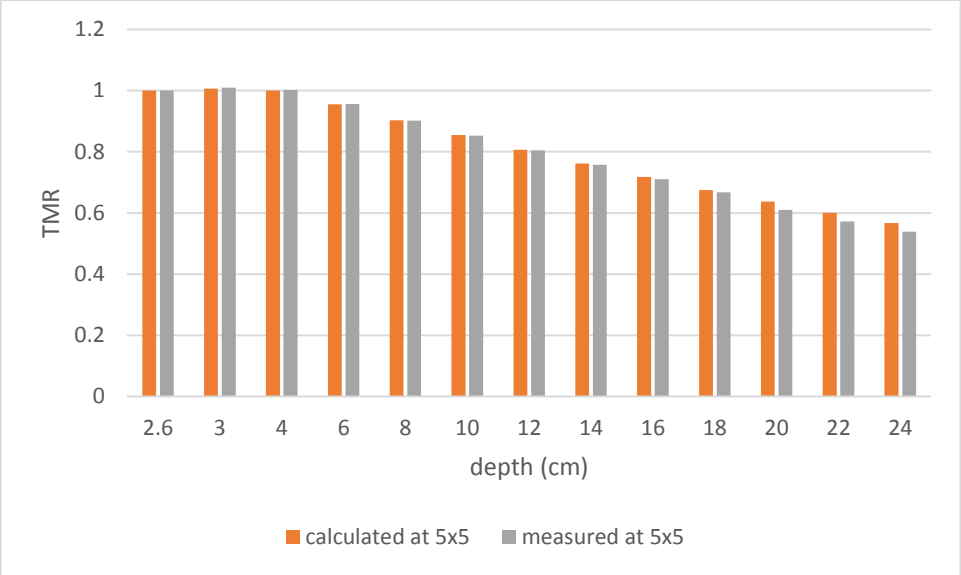

Figure 4.9: A graph of calculated and measured TMR against depth (cm) for 15 MV at 5x5 field sizes

From figure 4.9, the calculated and the measured TMRs showed good agreement from 2.6 cm to 18 cm after which there was a small disagreement. Comparing figure 4.7 with 4.9, at the same field size, it can be observed that for the high megavoltage beam (15 MV), the deviation of calculated TMR from the measured TMR started at deeper depth than that of the low megavoltage beam (6 MV).

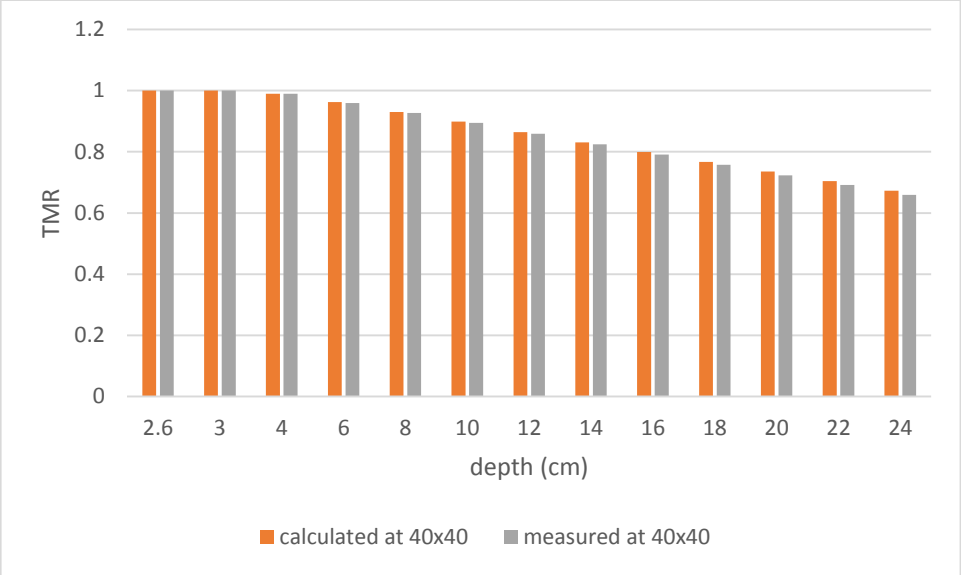

Figure 4.10: A graph of calculated and measured TMR against depth (cm) for 15 MV at 40x40 field sizes

From figure 4.10, it can also be seen that, both the calculated and the measured tissue maximum ratios (TMRs), had good agreement from 2.6 cm to 20 cm depth. This elaborate the fact that, for large field sizes and high energies, calculated TMR does not incorporate a significant error when used in monitor unit calculation.

4.1.3.1 Relative difference between calculated and measured TMR at different field sizes

Figure 4.11 below, depicts that the relative difference between the measured and the calculated tissue maximum ratios (TMRs) varies in direct proportional with depth for all field sizes at the 6 MV x-ray beam. Also at this 6 MV energy, the relative difference follows a good correlation for all field sizes.

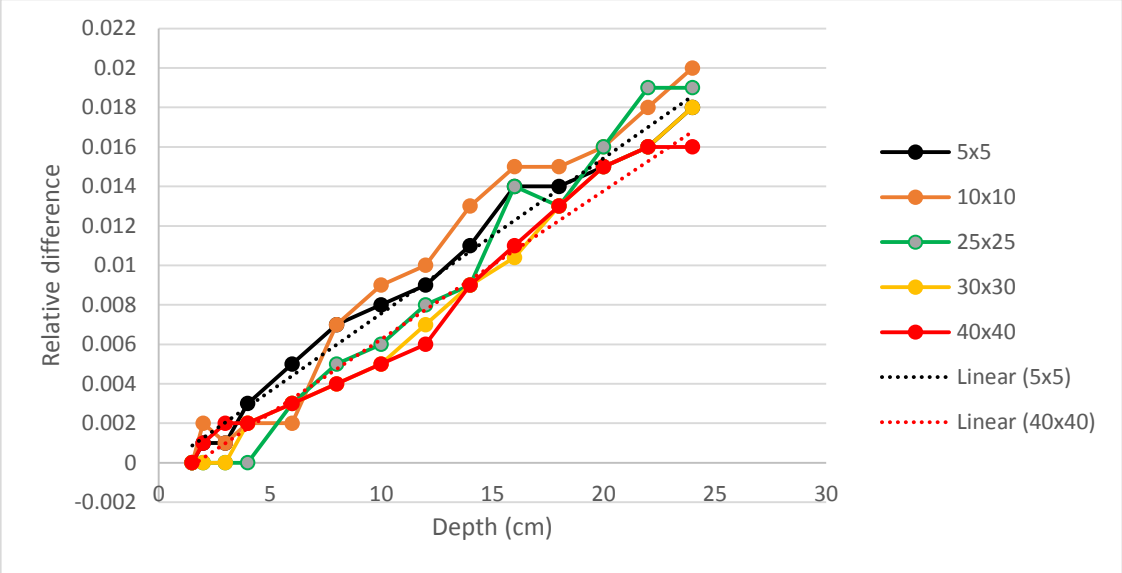

Figure 4.11: A graph of relative difference between calculated and measured TMR against depth (cm) for 6 MV

Again, there is a good agreement between the calculated tissue maximum ratio (TMR) and the measured TMR at lower depth but at higher depth, there is a significant deviation of the calculated TMR from the measured one. From the trend line drawn for the 5x5 cm and 40x40 cm, it can be seen that the large field size (40x40) showed an overall small relative difference between the calculated and the measured TMRs with depth. Of all the field sizes, a maximum percentage difference of 2.0 % was recorded for the 6 MV x-ray beam and this occurred at 10x10 cm field size whiles a minimum relative percentage difference of 1.6 % was recorded for the 6 MV x-ray beam, and this occurred at 40x40 cm field size.

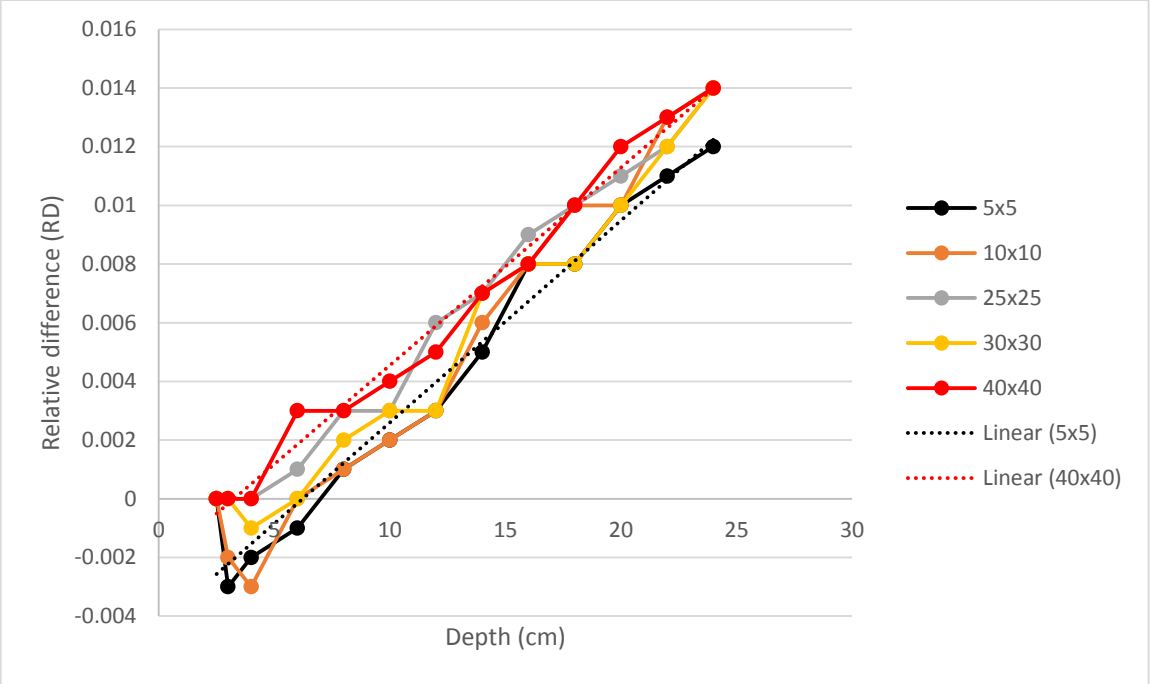

Figure 4.12: A graph of relative difference between calculated and measured TMR against depth (cm) for 15 MV

It can be seen from fig. 4.12 that, for a small field size (5x5), the relative difference between the calculated and the measured TMRs becomes higher than that of large field size (40x40) at lower depths of 3 cm and 4 cm. The large field sizes (40x40) and (25x25) had a zero relative difference between the calculated and the measured TMRs at lower depths 2.5 cm, 3 cm and 4 cm. In general, it can also be observed from fig. 4.12 that the relative differences between the calculated and the measured TMRs increase with depth for all field sizes. For all the field sizes in figure 4.12, a maximum percentage difference of 1.4 % was recorded whiles a minimum percentage difference of 1.2 % was recorded for the 15 MV x-ray beam, and these occurred at 40x40 cm and 5x5 cm respectively.

4.1.4 Verification of the Measured and the Calculated TMRs with that obtained during commission which is used on the Treatment Planning System.

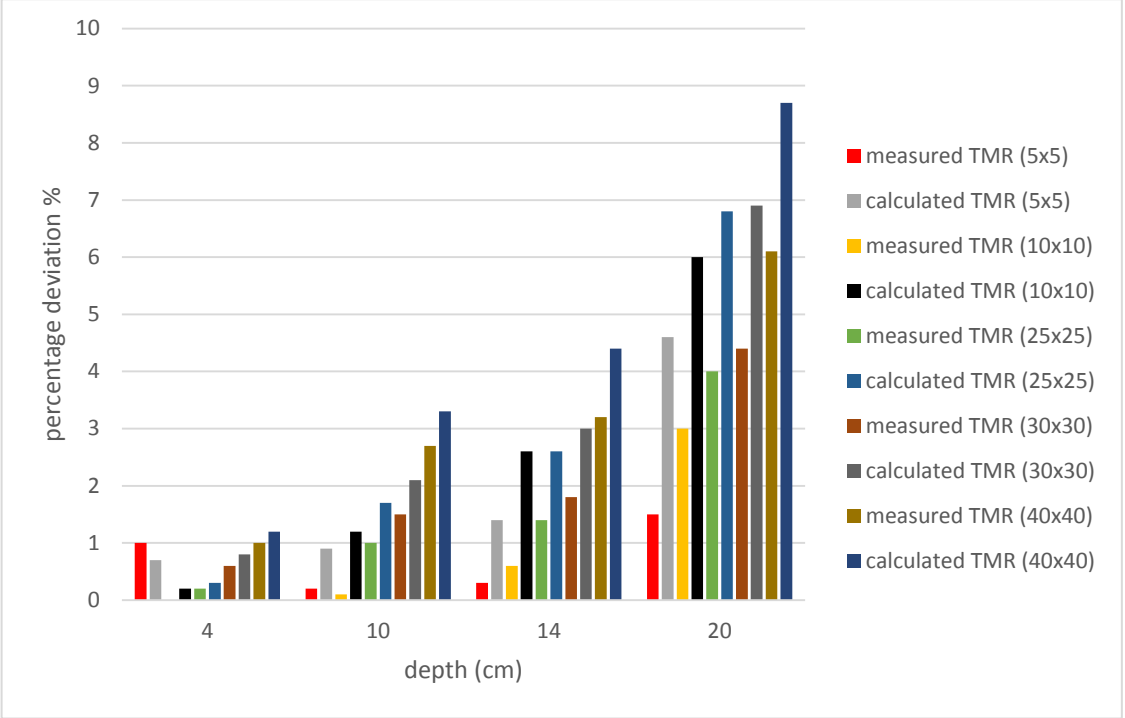

Figure 4.13 A graph of percentage deviations of both measured and calculated TMRs from that obtained during commission against depth for 6 MV

From fig. 4.13, it can be observed that at all depths except 4 cm and field sizes 5x5 cm, the calculated TMRs show higher percentage deviation from that obtained on TPS than that of the measured TMRs. Inferring from the graph, at a depth of 4 cm, the measured TMR for field size 10x10 cm recorded the minimum percentage deviation of 0 % and the calculated TMR for field size 40x40 cm at 20 cm depth recorded the highest deviation. Since from literature, a percentage deviation of 5 % is allowed in dose delivery, it can be confirmed that the measured TMR values agree well with that on the TPS at all depths except at 20 cm for 40x40 cm field size

whiles the calculated TMR recorded higher percentage deviation above 5 % at 20 cm from field size of 10x10 cm and beyond. A maximum percentage deviation of 8.7 % was recorded for the 6 MV.

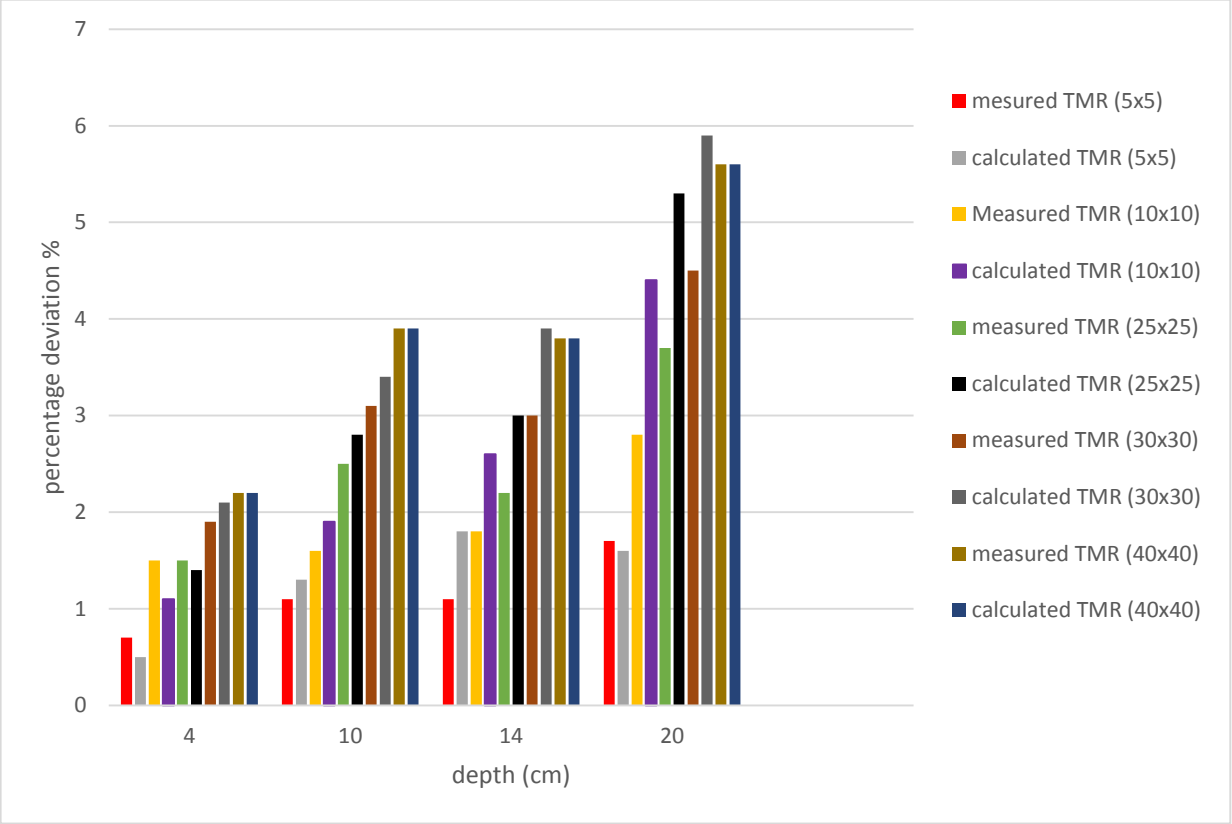

Figure 4.14 A graph of percentage deviations of both measured and calculated TMRs from that obtained during commission against depth for 15 MV

From fig. 4.14, at all depths, both the calculated and the measured TMRs recorded the smallest percentage deviation from that on the TPS for 5x5 cm field size. At 4 cm depth, the measured TMRs recorded higher deviations than calculated TMRs below 10x10 cm field. It could also be observed that, averagely, the percentage deviation

increases with field size and depth. Again, for large field size (40x40 cm), both the calculated and the measured TMRs were in good agreement, though they showed highest deviation from that on the treatment planning system. From fig. 4.14, the only measured TMR value which showed deviation above the 5 % (recommended tolerance from literature) was at 20 cm depth for 40x40 cm field size. A maximum percentage deviation of 5.6 % is observed for the 15 MV energy beam.

CHAPTER FIVE

CONCLUSIONS AND RECOMMENDATIONS

5.1 Conclusion

Percentage depth dose (PDD) and tissue maximum ratio (TMR) for the required field sizes and treatment depths were measured for 6 MV and 15 MV x-ray beam from the Elekta Synergy Platform linear accelerator unit at Sweden Ghana Medical Centre (SGMC). For the same field sizes and depths, tissue maximum ratios (TMRs) were also calculated from the measured percentage depth dose (PDD). The calculated tissue maximum ratios (TMRs) were compared with those of their measured counterpart, so as to check the validity of the formula used in converting PDD into TMR.

The results of the measured percentage depth dose (PDD), the measured TMR and the calculated TMR for 6 MV and 15 MV show that; for the same field size, both PDD and TMRs increase with energy of the photon beam, but decrease with depth in the phantom. The percentage dose reduction for the 6 MV photon beam is 2.74 % per cm, whiles the rate of percentage dose reduction for the 15 MV is 2.38 % per cm. The reference depth (depth of maximum dose, d_{max}) for the 6 MV photon beam occurred at 1.5 cm and that of 15 MV photon beam at 2.6 cm, which shows that reference depth of maximum dose (d_{max}) varies in direct proportion with energy of the photon beam.

In comparing the calculated TMR with the measured TMR, the results show that, for the same field size, the agreement between the calculated and the measured TMRs was enhanced with energy. The higher the energy, the smaller the deviation between the calculated the measured TMR.

For both 6 MV and 15 MV, the relative difference between the calculated and the measured TMRs varies linearly with depth for all field sizes. The minimum percentage differences recorded were 1.6 % for 40x40 cm field size and 1.2 % for 5x5 cm field size at 6 MV and 15 MV respectively, while the maximum percentage differences recorded were 2.0 % for 10x10 cm field size and 1.4 % for 40x40 cm at 6 MV and 15 MV x-ray beam respectively.

The calculated TMR has a favourable agreement with the measured counterpart at shallow depths for all field sizes and energy but at deeper depths, calculated TMR deviates significantly from the measured counterpart. Thus in using calculated TMR values in the treatment time calculation, for clinical use, care must be taken when using a large field size and higher megavoltage beam to treatment deep tumor.

The results from the treatment planning system testify that calculated TMRs above field size of 25x25 cm and depth 20 cm introduce significant error into the formula for converting PDD into TMR. It can generally be concluded that, the calculated data have been compared with the experimental measurements, and found to be in good agreement because, they are within the 2 % tolerance from literature.

5.2 Recommendations

The following are recommendations made to the various stake holders in the administration of dose to patient and also patient's protection against radiation.

5.2.1 Medical professionals

Based on the agreement between the measured and the calculated TMRs, the measured TMR data at SGMC and the calculation method can be used for double check during beam commission so as to check on the performance of the measuring system.

Also, it is recommended that, calculated tissue maximum ratio (TMR) can confidently be used in calculating monitor units especially when applying both large and small field sizes to treat shallow tumors for high megavoltage x-ray beam.

5.2.2 Sweden Ghana Medical Centre

Since there was slight deviation when the measured data was compared with that obtained on the treatment planning system during commission, it is recommended that comparison of the measured TMR and PDD with that obtained during commission, should be included in the annual quality assurance (QAs) of the machine.

5.2.3 Regulators

It is recommended that the Regulatory Authority (RA), monitors periodically, the dosimetry effectiveness, and conduct regular inspections on radiation and dosimetric equipment so as to ensure patient's safety and avoidance of overexposure or underexposure during the administration of radiation treatment.

5.2.4 Further research work

The study could be further extended by considering each energy with the addition of physical transmission factors such as wedge, bolus, tray and compare their calculated tissue maximum ratio (TMR) with their measured tissue maximum ratio (TMR)

REFERENCES

AAPM, (1983): A protocol for the determination of absorbed dose from high energy photon and electron beams. A report of Task Group 21, Radiation Therapy Committee. Medical physics, 10, 741-771.

Agawal K., Scheele R.V., and Wakley Jack. (1971). Tissue maximum-dose ratio (Tmr) for 8MV X-rays. Vol.112, No.4 page 797.

Anthink Hoog and Bernhard Christoph (2011); prediction of tumor definition for Image Guided Radiation Therapy. Thesis work at State University of New at York at Buffalo

Bagner F., "Physical aspect of super voltage x-ray therapy" Med. Phys.1, 266-274 (1974)

BJR, (1983): Central axis depth dose data for use in radiotherapy. British Journal of Radiology Supplement NO. 17., British Institute of Radiology, London.

BJR, (1996): Central axis depth dose data for use in radiotherapy. British Journal of Radiology Supplement no. 25., British Institute of Radiology, London

Bouno F. Joseph, R.T.T. (2010). Percentage depth dose (PDD) Beam on time and cord dose. Chapter 5. Allied Health Science Nassau Community College.

Brahme A. (editor) (1988): Accuracy Requirements and Quality Assurance of External Beam Therapy with Photons and Electrons. Acta Oncologica Supplementum 1, Stockholm.

Bruce R. Thomadsen, Shrikank S. Kubsad, Bhudah R. Paliwal Siamak Shahabi and T. Rockwell Mackie (1192). On the cause of variation with tissue-maximum ratio values with source to-detector distance. Med Phys. Vol.20, No. 3, page 723.

Cunningham J.R., Johns H.E., and Gupta S.K., Examination of definition and magnitude of back scatter factor for Cobalt 60 gamma rays. Brit. F. Radiol., 1965, 38, 637-639.

Das I. J., Cheng C. W., Watt J. R., Ahnesjo A., Gibbons J., Li A. X., Lowenstein J., Mitra K. R., Simon E. W. and Zhu C. Timothy (2008): Accelerator beam data commissioning equipment and procedures. Report of the TG-106 of then Therapy physics committee of the AAPM. Med. Phys. Vol. 35, No. 9

Dawson D.J., (1977) "Tissue-maximum ratios for high-energy x-rays" Med. Phys. 4. 423-430

Dawson, D. J. (1976): Percentage depth doses for high energy x-rays. Physics in medicine and biology, 21, 226-235.

Day, M. J. (1950): A note on the calculation of dose in x-ray fields. British Journal of Radiology, 23, 268-369.

DIN, (1990): Dosis mess verfahren nach der Sondenmethode fur photonen un d Elekronenstrah lung. DIN 6800 Teil 2 (draft).

Edward C. Halperin, Carlos A Prerez, Luther W. Brady (2008): Perez and Brady's Principles and Practice of Radiation Oncology; mitmycin C in anal cancer. Int. J Radiat Oncol. Biol. Phys. 72:119-126.

Edward C. Halperin, Carlos A. Perez, Luther Brady, (2008): Paraz and Brady's principles and practice of radiation therapy oncology, med. Phy., fifth edition, 156-165

ESTRO (2001), Monitor unit calculation for high energy photon beams. European Society for Radiotherapy and Oncology. Booklet 3, 1st Edition, Andree Dutreix, Bengt E. Bjarngard, Andre Bridier, Ben Mijnheer, Jim E. Shaw Hans Svensson.

Fermer C. Eghbali H, Meerwaldt J.H, Rieux C, Bosq J. Berger F. et al. Chemotherapy phys involved–field radiation in early stage Hodgkin's disease. N. Engl J. Med. 2007: 357: 1916-27.

Galvin, James M; Ezzell, Gary; Eisbrauch, Avraham; Yu, Cedric; Butler, Brian; Xiao, Ying; Rosen, Isaac; Rosenman, Julian; Sharpe, Michael; Xing, Lei; Xia, Ping; Lomax, Tony; Low, Daniel A; Palta, Jatinder (April 2004), "Implementing IMRT in clinical practice: a joint document of the American Society for Therapeutic Radiology and Oncology and the American Association of Physicists in Medicine.", *Int J Radiat Oncol Biol Phys.* **58** (5): 1616– 34.

Gamage N. J. W, Hill D. J. T, Lukey C. A, Pomery P. J., (2013): The use of high energy radiation as a probe for characterization of polyester melamine coating matrices.

Gersh J. A. (2014): The clinical impact of detector choice for scanning. Med. Phy. Vol. 15, No. 4. world wide web:http://jacmp.org. Retrieved on 28th March, 2015.

Holt J.G., Laughlin J.S., and Moroney J.P., Extension of Concept of tissue-air ratios (TAR) to high energy x-ray beams. Radiology 1970, 96, 437-446.

IAEA (1997): Quality Assurance in Radiotherapy. IAEA–TECDOC-1040. International Atomic Energy Agency, Vienna.

IAEA, (1987): Absorbed dose determination in photon and electron beam: and international code of practice IAEA Technical Report Series no. 227, (International Atomic Energy Agency, Vienna), pp. 1-98

IBA (2013): Detectors for relative and absolute dosimetry. world wide web:http://iba-dosimetry.com/product. Retrieved on 15th March, 2015

IBA (2014): Phantom for absolute dosimetry. IBA dosimetry, world wide web:http://iba-dosimetry.com. Retrieved on 15th July, 2014.

IBA (2015): Blue phantom^2-efficiency for LINAC commissioning and annual QA. world wide web:http://iba-dosimetry.com. Retrieved on 2nd May, 2015.

Johansson K.A., Hariot J.C., Van Dam J., Lepinoy D., SetenacI., Sernbo G. (1986): Quality assurance control in the EORTC cooperative group of radiotherapy. 2. Dosimetric intercomposition. Radiather, Oncol. 7,269-279.

Johns H. E., Whitmore G. F., Watson J. A. and Umberg F. H., (1953): A system of dosimetry for radiation therapy with typical rotation distributions, Journal of the Canadian Association of Radiologist, 4, 1-14.

Jones, D. E. A (1949): A note on backscatter and depth doses for elongated rectangular x-ray fields, British Journal of Radiology, 22, 342-345

Karabis A., Belloti P. and Baltas D.(2009): Optimization of Catheter Position and Dwell Time in Prostate HDR Brachytherapy using HIPO and Linear Programming WC in Med. Physics & Biomedical Eng., Vol. 25/I, pp. 612-615, Springer,

Karzmark C.K., Deubert A., and Leovinger R. Tissue-phantom ratio; aid to treatment planning. Brit.F. Radiol., 1965, 38, 158-159.

Khan F. M., (2012): the physics of radiation therapy: med. Phy. 4th edition, page 148-152.

Khan F.M. (1984): A system of dosimetric calculation in the Physics of Radiation Therapy 1st Edition, Williams and Wilkins, Baltimore, 182-204.

Kinsey E., Guerroro M., Prado K. and Yi B. – 2012. S.U.E.T-38: Are calculation methods for determining tissue maximum ratio from percentage depth dose valid for flattening filter-free photon beam? Med.phys.

Lahanas M, Baltas D, Giannouli S (2003) Global convergence analysis of fast multiobjective gradient-based dose optimization algorithms for high-dose-rate brachytherapy. Phys Med Biol 48:599-617

Lawrence T.S., Ten H.R.K., and Giaccia A. (2008). Principe of Radiation Oncology. 8th Edition. Lippincott Williams and Wilkins Press. Philaddpia.

Leon J. Erratum; interaction of radiation with matter: integrable problems. Phy Rev 1993; 48:2509.

Malhotra H., Wu V.,Wang Z., Patil S. (2012): A novel method for viginal cylinder treatment planning; a seamless transition to 3D brachytherapy. Med. Phys. Vol. 4(2); 92-100.

Marbach J.R and Almond P.R. (1977): Scattered photon as the cause for the observed d_{max} shift with field size in high energy photon beams. Med. Phys. 4, 310-314

Marinello G. and Dutriex A., "Etude Dosimetrique dun faisdeu de Rayons x de 25MV," J. Radiol. Electrik. 54, 951-958 (1973).

Mayneord W.V., and Lamerton L.F. (1941): Survey of depth dose data. Brit F. Radiol. 14, 255-264.

Padikal T. N. and Deye J. A. (1978): electron contamination of a high energy x-ray beam, 'Phys. Med. Biol. 23, 1086-1092.

Podgorsak (2006) E.B.. External Photon Beams; Physic aspects chapter 6 page 169

Potomaki L. K. (1968): The equivalent field principles and its use in beam therapy dose calculations. British Journal of radiology, 41, 381-383.

Purdy J. A (1996): Intensity modulated radiation therapy, Int. J Radiat oncol, Biol. Phy. (4), 845-846

RT Answers (2009). Treatment types: Stereotactic Radiation Therapy. Retrieved on 20th May, 2014 from the world wide web:http://rtanswers.com.

Saeed Ahmad Buzdar, Muhammed Afsal Rao, Aalia Nazor, 2009 Analysis of depth dose characteristics of photon in water

Samulski T., Dubuque G.L., Cacak R.K., Courlas G., Dewerd L.A., Hilko R., Humphries L., Jones D., Masterson M.E., Miller D. W., Stovall M., Wochos J.F. (1981): Radiation therapy dosimetry reviews by the centres for radiological physics. Int. J. Radiat. Oncol. Biol. Phys. 7, 379-383.

SPUNEL M., MIHAI M., MALAESCU I. 2013 on: experimental results in percentage depth dose (pdd) determination at the extended distances.

Sterling T. D., Perry H. and Katz, L,(1964): Automation of radiation treatment planning. 1v. Derivation of mathematical expression for the percentage depth dose of cobalt-60 beams and visualization of multiple field dose distribution, British Journal of Radiology.

Subramania Jayaraman and Lawrence H. Lanzl, (2011): clinical radiotherapy physics, med. Phy. Second edition, 200-228.

Wambersie A., Van Dam J., Hanks G., Mijnheer B.J., Battermann J.J. (994): What accuracy is needed in dosimetry? IAEA,-TECDOC 734. IAEA, Vienna, 11-35.

Wegner R.E. (2011): Stereotactic radiosurgery for patients with brain metastases. Int. J. Radial. Biol. Phys. 3, 21-7.

Welkley D.E., Mnason D.J., Purdy J.A. and Oliver Jr. G.D., "Build-up region of megavoltage photon radiation source: Med. Phys. 2, 14-19 (1975).

Wellhofer Dosimetrie GmbH (2001): The blue phantom manual. IBA advanced radiotherapy. world wide web:http://iba.ar.com. Retrieved on 10th November, 2014

WHO (2008): Radiotherapy risk profile. Technical manual. World Health Organisation. Geneva.

Worthley B. (1996): equivalent squares of rectangular fields. British Journal of Radiology, 39, 559

Zhang Guang-shun, Huang Shao-min, Chen Cui, Xu Sen-kui, Zhang Dan-dan and Deng Xiao-wu, (2014): Evaluating the therapeutic dose distribution of intensity modulated radiation therapy for head and neck with cone-beam computer tomography image; A methodological image, Bio. Med.

APPENDIX

Appendix A Measured Percentage Depth Dose (PDD) data for 6MV x-ray beam

Depth (cm)	Squared field size (cm^2)										
	25	**36**	**49**	**64**	**100**	**144**	**225**	**400**	**625**	**900**	**1600**
1.5	100.0	100.0	100.0	100.0	100.0	100.0	100.0	100.0	100.0	100.0	100.0
2	99.6	99.5	99.6	99.4	99.4	99.4	99.2	99.1	99.0	98.9	98.9
3	95.2	95.3	95.5	95.5	95.7	95.5	95.5	95.5	95.4	95.4	95.8
4	90.5	90.6	91.0	91.2	91.4	91.5	91.6	91.9	91.7	92.0	92.3
5	85.9	86.2	86.6	86.7	87.3	87.5	87.8	88.0	88.1	88.4	88.9
6	81.3	81.7	82.3	82.7	83.2	83.6	84.0	84.4	84.6	84.9	85.5
7	77.0	77.4	78.0	78.5	79.2	79.8	80.2	80.8	81.2	81.5	82.2
8	72.7	73.1	74.0	74.5	75.3	76.0	76.6	77.4	77.8	78.3	78.9
9	68.6	69.3	70.0	70.7	71.6	72.4	73.1	73.9	74.5	75.1	75.7
10	64.8	65.5	66.3	66.9	68.0	68.9	69.7	70.6	71.3	71.8	72.6
11	61.1	61.9	62.7	63.4	64.5	65.4	66.3	67.4	68.2	68.8	69.8
12	57.6	58.4	59.3	60.1	61.2	62.2	63.2	64.4	65.2	65.8	66.8
13	54.4	55.3	56.1	56.9	58.1	59.0	60.1	61.4	62.2	63.0	64.1
14	51.2	52.2	53.1	53.7	55.1	56.1	57.3	58.5	59.4	60.2	61.3
15	48.4	49.3	50.1	51.0	52.3	53.3	54.4	55.8	56.8	57.6	58.7
16	45.7	46.5	47.5	48.3	49.5	50.5	51.8	53.1	54.3	55.0	56.2
17	43.2	44.0	44.8	45.6	46.9	47.9	49.2	50.7	51.7	52.5	53.7
18	40.6	41.6	42.4	43.2	44.4	45.5	46.7	48.4	49.3	50.2	51.4
19	38.4	39.2	40.1	40.8	42.2	43.3	44.4	46.0	47.1	48.0	49.2
20	36.3	37.1	38.0	38.6	39.8	40.9	42.2	43.8	44.9	45.8	47.0
21	34.3	35.1	35.9	36.6	37.8	38.9	40.1	41.7	42.9	43.7	45.0
22	32.3	33.1	33.9	34.6	35.8	36.9	38.1	39.7	40.9	41.7	43.0
23	30.6	31.3	32.1	32.8	34.0	35.0	36.2	37.8	38.9	39.8	41.1
24	28.9	29.6	30.3	31.0	32.2	33.2	34.4	36.0	37.1	38.0	39.2
25	27.3	28.0	28.7	29.4	30.5	31.5	32.7	34.2	35.4	36.2	37.5

Appendix B Measured Percentage Depth Dose (PDD) data for 15MV x-ray beam

Depth (cm)	Squared field size (cm^2)										
	25	**36**	**49**	**64**	**100**	**144**	**225**	**400**	**625**	**900**	**1600**
2.6	100.0	100.0	100.0	100.0	100.0	100.0	100.0	100.0	100.0	100.0	100.0
3.0	99.8	100	100	99.9	98.8	99.5	99.3	99.2	99.2	99.2	99.2
4.0	97.3	97.5	97.4	97.3	97.1	96.6	96.6	96.3	96.3	96.1	96.4
5.0	93.5	93.6	93.6	93.7	93.4	93.3	93.0	92.8	92.9	92.9	93.3
6.0	89.5	89.6	89.8	89.7	89.8	89.5	89.6	89.5	89.6	89.6	90.1
7.0	85.5	85.8	86.1	86.2	86.2	86	86.3	86.3	86.4	86.5	86.9
8.0	81.5	82.0	82.4	82.4	82.6	82.7	82.9	82.9	83.2	83.4	83.9
9.0	78.1	78.5	78.8	79	79.1	79.3	79.6	79.8	80.1	80.3	80.9
10.0	74.4	74.9	75.3	75.5	75.9	76.0	76.5	76.8	77.2	77.4	78.1
11.0	71.1	71.6	72	72.2	72.6	72.9	73.4	73.8	74.3	74.6	75.2
12.0	67.7	68.2	68.8	69.1	69.6	69.9	70.4	70.8	71.5	71.8	72.5
13.0	64.6	65.3	65.9	66.1	66.7	67.1	67.7	68.2	68.8	69.1	69.9
14.0	61.7	62.3	62.9	63.2	63.9	64.2	64.9	65.5	66.0	66.6	67.3
15.0	58.8	59.4	60	60.5	61.1	61.5	62.2	62.9	63.6	64.0	64.8
16.0	56.2	56.7	57.3	57.7	58.4	58.9	59.6	60.4	61.1	61.7	62.5
17.0	53.6	54.2	54.8	55.2	56.0	56.4	57.2	58	58.7	59.3	60.2
18.0	51.0	51.8	52.4	52.7	53.6	54.0	54.8	55.7	56.5	57.0	58.0
19.0	48.8	49.5	50.0	50.5	51.3	51.8	52.7	53.5	54.3	54.9	55.8
20.0	46.6	47.1	47.9	48.2	49.0	49.6	50.4	51.4	52.1	52.7	53.7
21.0	44.5	45.1	45.6	46.1	47.0	47.5	48.3	49.3	50.1	50.7	51.7
22.0	42.5	43.0	43.7	44.1	45.0	45.6	46.5	47.3	48.1	48.8	49.8
23.0	40.6	41.1	41.8	42.1	43.0	43.6	44.5	45.5	46.4	46.9	47.8
24.0	38.8	39.3	39.9	40.3	41.2	41.8	42.7	43.7	44.5	45.1	46.1
25.0	37.0	37.6	38.2	38.6	39.4	40.0	40.8	41.9	42.7	43.3	44.4

Appendix C Measured Tissue Maximum Ratio (TMR) data for 6MV x-ray beam

	Squared field size (cm^2)										
Depth (cm)	25	36	49	64	100	144	225	400	625	900	1600
1.5	1.000	1.000	1.000	1.000	1.000	1.000	1.000	1.000	1.000	1.000	1.000
2.0	1.005	1.005	1.004	1.004	1.002	1.002	1.000	0.999	1.000	0.999	0.998
3.0	0.979	0.979	0.981	0.982	0.984	0.982	0.982	0.982	0.982	0.982	0.985
4.0	0.947	0.949	0.952	0.956	0.958	0.959	0.960	0.962	0.963	0.964	0.967
5.0	0.915	0.920	0.923	0.926	0.931	0.933	0.937	0.939	0.941	0.944	0.949
6.0	0.882	0.888	0.893	0.899	0.905	0.908	0.912	0.916	0.920	0.923	0.929
7.0	0.849	0.856	0.861	0.867	0.875	0.881	0.887	0.893	0.899	0.903	0.910
8.0	0.816	0.823	0.830	0.838	0.846	0.854	0.861	0.870	0.876	0.882	0.889
9.0	0.782	0.793	0.800	0.807	0.819	0.827	0.836	0.845	0.854	0.861	0.869
10.0	0.753	0.763	0.770	0.778	0.790	0.800	0.811	0.822	0.831	0.838	0.848
11.0	0.721	0.732	0.740	0.748	0.763	0.773	0.785	0.797	0.808	0.816	0.828
12.0	0.692	0.703	0.711	0.719	0.735	0.746	0.760	0.775	0.786	0.794	0.807
13.0	0.663	0.675	0.684	0.692	0.709	0.720	0.733	0.749	0.762	0.771	0.786
14.0	0.635	0.647	0.657	0.666	0.682	0.694	0.710	0.727	0.740	0.750	0.764
15.0	0.608	0.622	0.631	0.640	0.657	0.670	0.686	0.703	0.717	0.729	0.743
16.0	0.583	0.596	0.605	0.616	0.632	0.645	0.661	0.679	0.695	0.708	0.723
17.0	0.559	0.572	0.582	0.590	0.607	0.621	0.637	0.657	0.673	0.686	0.701
18.0	0.535	0.548	0.558	0.567	0.585	0.598	0.615	0.636	0.653	0.665	0.682
19.0	0.515	0.526	0.535	0.544	0.562	0.576	0.594	0.614	0.632	0.646	0.663
20.0	0.492	0.505	0.513	0.523	0.540	0.552	0.571	0.593	0.612	0.625	0.642
21.0	0.470	0.484	0.493	0.503	0.520	0.533	0.551	0.572	0.591	0.606	0.624
22.0	0.451	0.463	0.473	0.482	0.499	0.512	0.531	0.553	0.572	0.586	0.605
23.0	0.434	0.445	0.453	0.462	0.481	0.493	0.511	0.533	0.553	0.567	0.586
24.0	0.413	0.426	0.436	0.444	0.461	0.473	0.492	0.515	0.534	0.549	0.569
25.0	0.397	0.408	0.418	0.426	0.443	0.456	0.474	0.497	0.516	0.531	0.550

Appendix D Measured Tissue Maximum Ratio (TMR) data for 15MV x-ray beam

	Squared field size (cm^2)										
Depth (cm)	**25**	**36**	**49**	**64**	**100**	**144**	**225**	**400**	**625**	**900**	**1600**
2.5	1.000	1.000	1.000	1.000	1.000	1.000	1.000	1.000	1.000	1.000	1.000
3.0	1.009	1.010	1.012	1.009	1.008	1.005	1.002	1.000	1.000	1.000	1.000
4.0	1.002	1.004	1.004	1.002	1.001	0.995	0.993	0.990	0.989	0.988	0.990
5.0	0.980	0.982	0.983	0.982	0.979	0.977	0.975	0.972	0.972	0.973	0.976
6.0	0.956	0.957	0.960	0.959	0.959	0.956	0.956	0.955	0.955	0.956	0.959
7.0	0.930	0.933	0.936	0.938	0.939	0.937	0.937	0.937	0.938	0.940	0.944
8.0	0.902	0.907	0.913	0.913	0.914	0.915	0.916	0.917	0.919	0.922	0.927
9.0	0.878	0.885	0.889	0.890	0.893	0.893	0.896	0.898	0.901	0.905	0.910
10.0	0.853	0.858	0.863	0.866	0.870	0.872	0.876	0.880	0.884	0.887	0.894
11.0	0.828	0.835	0.840	0.843	0.847	0.850	0.854	0.859	0.865	0.870	0.875
12.0	0.804	0.809	0.815	0.819	0.826	0.830	0.834	0.839	0.846	0.853	0.859
13.0	0.779	0.786	0.794	0.799	0.805	0.809	0.816	0.822	0.828	0.835	0.842
14.0	0.757	0.764	0.771	0.774	0.783	0.788	0.794	0.802	0.808	0.815	0.824
15.0	0.734	0.740	0.747	0.752	0.762	0.767	0.774	0.783	0.791	0.798	0.807
16.0	0.710	0.720	0.726	0.730	0.739	.0746	0.754	0.763	0.772	0.781	0.791
17.0	0.689	0.698	0.705	0.710	0.719	0.726	0.734	0.745	0.754	0.763	0.774
18.0	0.667	0.675	0.684	0.690	0.699	0.707	0.715	0.727	0.737	0.746	0.757
19.0	0.649	.0.657	0.665	0.669	0.680	0.688	0.697	0.709	0.720	0.729	0.741
20.0	0.610	0.637	0.644	0.650	0.660	0.669	0.678	0.690	0.702	0.711	0.723
21.0	0.590	0.618	0.625	0.630	0.642	0.650	0.660	0.673	0.685	0.695	0.707
22.0	0.572	0.599	0.606	0.612	0.623	0.630	.643	0.657	0.668	0.678	0.691
23.0	0.555	0.581	0.589	0.594	0.605	0.613	0.625	0.639	0.652	0.663	0.675
24.0	0.539	0.564	0.571	0.576	0.588	0.598	0.608	0.623	0.636	0.645	0.659
25.0	0.517	0.547	0.555	0.560	0.571	0.580	.591	0.605	0.619	0.630	0.643

Appendix E Calculated Tissue Maximum Ratio (TMR) data for 6 MV x-ray beam

Squared field size (cm^2)

Depth	5x5	6x6	7x7	8x8	10x10	12x12	15x15	20x20	25x25	30x30	40x40
1.5	1.000	1.000	1.000	1.000	1.000	1.000	1.000	1.000	1.000	1.000	1.000
2.0	1.006	1.005	1.006	1.004	1.004	1.004	1.002	1.001	1.000	0.999	0.999
3.0	0.980	0.981	0.983	0.983	0.985	0.983	0.983	0.983	0.982	0.982	0.987
4.0	0.950	0.951	0.955	0.957	0.960	0.961	0.962	0.965	0.963	0.966	0.969
5.0	0.919	0.922	0.927	0.928	0.934	0.936	0.940	0.942	0.943	0.946	0.951
6.0	0.887	0.891	0.898	0.902	0.907	0.912	0.916	0.920	0.923	0.926	0.932
7.0	0.856	0.860	0.867	0.872	0.880	0.887	0.891	0.898	0.902	0.906	0.913
8.0	0.823	0.828	0.838	0.843	0.853	0.860	0.867	0.876	0.881	0.886	0.893
9.0	0.791	0.799	0.807	0.815	0.826	0.835	0.843	0.852	0.859	0.866	0.873
10.0	0.761	0.769	0.779	0.786	0.799	0.809	0.819	0.829	0.837	0.843	0.853
11.0	0.731	0.740	0.750	0.758	0.771	0.782	0.793	0.806	0.816	0.823	0.835
12.0	0.701	0.711	0.722	0.732	0.745	0.757	0.770	0.784	0.794	0.801	0.813
13.0	0.674	0.685	0.695	0.705	0.720	0.731	0.745	0.761	0.771	0.781	0.794
14.0	0.646	0.658	0.670	0.677	0.695	0.708	0.723	0.738	0.749	0.759	0.773
15.0	0.621	0.633	0.643	0.655	0.671	0.684	0.698	0.716	0.729	0.739	0.754
16.0	0.597	0.607	0.620	0.631	0.647	0.660	0.677	0.694	0.709	0.718	0.734
17.0	0.574	0.585	0.595	0.606	0.623	0.636	0.654	0.674	0.687	0.698	0.714
18.0	0.549	0.562	0.573	0.584	0.600	0.615	0.631	0.654	0.666	0.678	0.695
19.0	0.528	0.539	0.551	0.561	0.580	0.595	0.610	0.632	0.647	0.660	0.676
20.0	0.507	0.519	0.531	0.540	0.556	0.572	0.590	0.612	0.628	0.640	0.657
21.0	0.487	0.499	0.510	0.520	0.537	0.553	0.570	0.593	0.610	0.621	0.640
22.0	0.467	0.478	0.490	0.500	0.517	0.533	0.550	0.574	0.591	0.602	0.621
23.0	0.449	0.460	0.471	0.482	0.499	0.514	0.532	0.555	0.571	0.584	0.604
24.0	0.431	0.442	0.452	0.463	0.481	0.496	0.513	0.537	0.554	0.567	0.585
25.0	0.414	0.425	0.435	0.446	0.463	0.478	0.496	0.519	0.537	0.549	0.569

Appendix F Calculated Tissue Maximum Ratio (TMR) data for 15 MV x-ray beam

depth	5x5	6x6	7x7	8x8	10x10	12x12	15x15	20x20	25x25	30x30	40x40
2.6	1.000	1.000	1.000	1.000	1.000	1.000	1.000	1.000	1.000	1.000	1.000
3.0	1.006	1.008	1.008	1.007	1.006	1.003	1.001	1.000	1.000	1.000	1.000
4.0	1.000	1.002	1.001	1.000	0.998	0.993	0.993	0.989	0.989	0.987	0.990
5.0	0.979	0.980	0.980	0.981	0.978	0.977	0.974	0.972	0.973	0.973	0.977
6.0	0.955	0.956	0.959	0.957	0.959	0.955	0.956	0.955	0.956	0.956	0.962
7.0	0.930	0.933	0.936	0.938	0.938	0.935	0.939	0.939	0.940	0.941	0.945
8.0	0.903	0.909	0.913	0.913	0.915	0.916	0.919	0.919	0.922	0.924	0.930
9.0	0.881	0.886	0.889	0.892	0.893	0.895	0.898	0.901	0.904	0.906	0.913
10.0	0.855	0.861	0.866	0.868	0.872	0.874	0.879	0.883	0.887	0.890	0.898
11.0	0.832	0.838	0.843	0.845	0.850	0.853	0.859	0.864	0.870	0.873	0.880
12.0	0.807	0.813	0.820	0.823	0.829	0.833	0.839	0.844	0.852	0.856	0.864
13.0	0.784	0.792	0.799	0.802	0.809	0.814	0.821	0.827	0.835	0.838	0.848
14.0	0.762	0.769	0.777	0.780	0.789	0.793	0.801	0.809	0.815	0.822	0.831
15.0	0.739	0.746	0.754	0.760	0.768	0.773	0.781	0.790	0.799	0.804	0.814
16.0	0.718	0.725	0.732	0.738	0.747	0.753	0.762	0.772	0.781	0.789	0.799
17.0	0.697	0.705	0.713	0.718	0.728	0.733	0.744	0.754	0.763	0.771	0.783
18.0	0.675	0.685	0.693	0.697	0.709	0.714	0.725	0.737	0.747	0.754	0.767
19.0	0.656	0.666	0.673	0.679	0.690	0.697	0.709	0.720	0.730	0.739	0.751
20.0	0.637	0.644	0.655	0.659	0.670	0.678	0.689	0.703	0.713	0.721	0.735
21.0	0.619	0.627	0.634	0.641	0.654	0.661	0.672	0.686	0.697	0.705	0.719
22.0	0.601	0.608	0.618	0.624	0.636	0.645	0.657	0.669	0.680	0.690	0.704
23.0	0.584	0.591	0.601	0.605	0.618	0.627	0.640	0.654	0.667	0.674	0.687
24.0	0.567	0.574	0.583	0.589	0.602	0.611	0.624	0.638	0.650	0.659	0.673
25.0	0.549	0.558	0.567	0.573	0.585	0.594	0.606	0.622	0.634	0.643	0.659

Squared field size (cm^2)

Appendix G Doses obtained from TPS, calculated and Measured TMR for 6 MV

Squared field size (cm^2)

depth (cm)	5x5 Dose (Gy) at isocentre from			10x10 Dose (Gy) at isocentre from			25x25 Dose (Gy) at isocentre from			30x30 Dose (Gy) at isocentre from			40x40 Dose (Gy) at isocentre from		
	TPS	Measure TMR	Calculated TMR	TPS	Measure TMR	Calculated TMR	TPS	Measure TMR	Calculated TMR	TPS	Measure TMR	Calculated TMR	TPS	Measure TMR	Calculated TMR
4	10	9.9	9.93	10	10	10.02	10	10.02	10.03	10	10.06	10.08	10	10.1	10
10	10	9.98	10.09	10	10.01	10.12	10	10.1	10.17	10	10.15	10.21	10	10.27	10
14	10	9.97	10.14	10	10.06	10.26	10	10.14	10.26	10	10.18	10.3	10	10.32	10
20	10	10.2	10.46	10	10.3	10.6	10	10.4	10.68	10	10.44	10.69	10	10.61	11

Relative percentage deviation of TMR doses from that of the TPS

depth (cm)	5x5 Measure TMR	5x5 Calculated TMR	10x10 Measure TMR	10x10 Calculated TMR	25x25 Measure TMR	25x25 Calculated TMR	30x30 Measure TMR	30x30 Calculated TMR	40x40 Measure TMR	40x40 Calculated TMR
4	1	0.7	0	0.2	0.2	0.3	0.6	0.8	1	1.2
10	0.2	0.9	0.1	1.2	1	1.7	1.5	2.1	2.7	3.3
14	0.3	1.4	0.6	2.6	1.4	2.6	1.8	3	3.2	4.4
20	1.5	4.6	3	6	4	6.8	4.4	6.9	6.1	8.7

Appendix H Doses obtained from TPS, calculated and Measured TMR for 15 MV

Equivalent square field (cm^2)															
depth (cm)	5x5 Dose (Gy) at isocentre from			10x10 Dose (Gy) at isocentre from			25x25 Dose (Gy) at isocentre from			30x30 Dose (Gy) at isocentre from			40x40 Dose (Gy) at isocentre from		
	TPS	Measure TMR	Calculated TMR	TPS	Measure TMR	Calculated TMR	TPS	Measure TMR	Calculated TMR	TPS	Measure TMR	Calculated TMR	TPS	Measure TMR	Calculated TMR
4	10	10.1	10.05	10	10.15	10.11	10	10.15	10.14	10	10.19	10.21	10	10.22	10
10	10	10.1	10.13	10	10.16	10.19	10	10.25	10.28	10	10.31	10.34	10	10.39	10
14	10	10.1	10.18	10	10.18	10.26	10	10.22	10.3	10	10.3	10.39	10	10.38	10
20	10	10.2	10.16	10	10.28	10.44	10	10.37	10.53	10	10.45	10.59	10	10.56	11
Relative percentage deviation of TMR doses from that of the TPS															
depth (cm)	5x5 Measure TMR		5x5 Calculated TMR	10x10 Measure TMR		10x10 Calculated TMR	25x25 Measure TMR		25x25 Calculated TMR	30x30 Measure TMR		30x30 Calculated TMR	40x40 Measure TMR		40x40 Calculated TMR
4	0.7		0.5	1.5		1.1	1.5		1.4	1.9		2.1	2.2		2.2
10	1.1		1.3	1.6		1.9	2.5		2.8	3.1		3.4	3.9		3.9
14	1.1		1.8	1.8		2.6	2.2		3.0	3.0		3.9	3.8		3.8
20	1.7		1.6	2.8		4.4	3.7		5.3	4.5		5.9	5.6		5.6